

RESEARCH

Open Access



Proteasome inhibition enhances oncolytic reovirus therapy in multiple myeloma independently of its direct cytotoxic effects

Ada Alice Dona^{1,2†}, Theophilus Tandoh^{1,2†}, Lokesh Nigam^{1,2†}, Mahmoud Singer^{1,2}, Enrico Caserta^{1,2}, Mariam Murtadha^{1,2}, Yinghui Zhu^{1,2}, Milad Moloudizargari^{1,2}, Preeti Sharma^{1,2}, Ottavio Napolitano^{1,2}, Janet Winchester^{1,2}, Arnab Chowdhury^{1,3}, Alex Pozhitkov^{1,2}, James F. Sanchez¹, Hawa Vahed^{1,2}, Guido Marcucci², Matt Coffey⁴, Gerard Nuovo⁵, Douglas W. Sborov^{6*}, Flavia Pichiorri^{1,2*} and Craig C Hofmeister^{7*}

Abstract

Background Reovirus (RV) is an oncolytic virus with natural tropism for cancer cells. We previously showed that RV administration in multiple myeloma (MM) patients was safe, but disease control associated with viral replication in the cancer cells was not observed. The combination with proteasome inhibitors (PIs) has shown to enhance RV therapeutic activity, but the mechanisms of action have not been fully elucidated.

Methods Electron microscopy, q-RT-PCR, single-cell mass cytometry (CyTOF), flow cytometry, plaque assays, immunohistochemistry, and Western blot analysis were used to assess RV infection of both myeloma and immune cells. Immune fluorescence, flow cytometry, and luciferase reporter assays were used to assess NF- κ B pathway activation upon RV treatments. Immune profiling changes, both ex vivo and in MM patients, were analyzed by flow cytometry and CyTOF analysis. T-cell receptor (TCR) sequencing was also conducted both in immune competent MM mice and in patients enrolled in a phase 1b trial per a standard 3 + 3 dose escalation schedule.

Results Here we show ex vivo and in vivo that proteasome inhibitors (PIs) potentiate reovirus replication in circulating classical monocytes, increasing viral delivery to myeloma cells. We found that the anti-viral signals in monocytes primarily rely on NF- κ B activation and that this effect is impaired by the addition of PIs. Conversely, the addition of PIs to RV therapy supports immune activation and killing of MM, independently of direct PI sensitivity. To validate the importance of PIs in enhancing oncolytic viral therapy independently of their killing activity on cancer cells, we then conducted a phase 1b trial of the reovirus Pelareorep together with the PI carfilzomib in 13 heavily

[†]Ada Alice Dona, Theophilus Tandoh and Lokesh Nigam contributed equally to this work.

*Correspondence:
Douglas W. Sborov
douglas.sborov@hci.utah.edu
Flavia Pichiorri
fpichiorri@coh.org
Craig C Hofmeister
craig.hofmeister@emory.edu

Full list of author information is available at the end of the article



© The Author(s) 2024. **Open Access** This article is licensed under a Creative Commons Attribution-NonCommercial-NoDerivatives 4.0 International License, which permits any non-commercial use, sharing, distribution and reproduction in any medium or format, as long as you give appropriate credit to the original author(s) and the source, provide a link to the Creative Commons licence, and indicate if you modified the licensed material. You do not have permission under this licence to share adapted material derived from this article or parts of it. The images or other third party material in this article are included in the article's Creative Commons licence, unless indicated otherwise in a credit line to the material. If material is not included in the article's Creative Commons licence and your intended use is not permitted by statutory regulation or exceeds the permitted use, you will need to obtain permission directly from the copyright holder. To view a copy of this licence, visit <http://creativecommons.org/licenses/by-nc-nd/4.0/>.

pretreated PI-resistant MM patients. Objective responses, which were associated with active reovirus replication in MM cells, T cell activation, and monocytic expansion, were noted in 70% of patients.

Conclusions Although characterized as immunosuppressive drugs, PIs improved RV delivery to MM cells but also enhanced anti-MM efficacy through immune-mediated killing of myeloma cells, independently of their PI sensitivity. These results highlight a more generalizable use of PIs as therapeutic companions to support oncolytic-based therapies in cancers.

Trial registration clinicaltrials.gov, NCT 02101944.

Keywords Proteasome inhibitors, Multiple myeloma, Oncolytic therapy, Reovirus, Mass cytometry, Monocytes

Background

Oncolytic viruses preferentially target and kill cancer cells without destroying normal cells. Talimogene laherparepvec (TVEC), the first FDA-approved oncolytic virotherapy, is a modified herpes simplex virus-1 (HSV-1) that encodes granulocyte-macrophage colony-stimulating factor (GM-CSF) and is now used for the treatment of metastatic melanoma [1]. Although oncolytic viruses for patients with solid tumors have primarily been injected in a specific tumor mass, successful treatment of a hematologic malignancy with an oncolytic virus requires intravenous infusion to transport the virus through the bloodstream to the bone marrow (BM) or extramedullary sites of disease to infect cancer cells and lead to cancer cell death, either through direct cytolysis or by engaging the immune microenvironment.

Reovirus Serotype 3 - Dearing Strain (RV) is a ubiquitous, non-enveloped, double-stranded RNA virus [2] that can cause mild gastroenteritis, coughing, and various flu-like symptoms [3]; it has been implicated in the initiation of celiac disease by promoting the loss of tolerance to dietary antigens [4]. The therapeutic form of RV, Pelareorep, was granted orphan drug status by the FDA and has been infused intravenously in numerous clinical trials. It exerts anti-neoplastic effects through both apoptotic and non-apoptotic mechanisms [5]. Due to RV's natural tropism for transformed cells and its relatively non-pathogenic profile, it is considered an ideal non-engineered virus for oncolytic therapy [6, 7].

RV entry into cells requires sequential binding, first to extracellular sialic acid followed by engagement of junctional adhesion molecule A (JAM-A) [8–10], a receptor that is expressed on the surface of multiple myeloma (MM) cells [11, 12]. RV is capable of selectively replicating in transformed cells with impaired intracellular antiviral responses, leading to selective anti-tumor activity [13, 14]. Preclinical investigation of RV for the treatment of MM has demonstrated significant anti-MM effects *in vitro* and *in vivo* when used as a single agent and in combination with proteasome inhibitors (PIs) and histone deacetylase inhibitors [15, 16], but proposed mechanisms associated with the anti-MM activity of RV in combination with these agents have been unclear. Our

initial trial, the first investigation of RV in any hematologic malignancy, used intravenous RV as a single agent in relapsed MM [17]. This trial showed that RV was able to reach MM cells in the marrow; however, it was unable to induce a productive infection or confer disease control through cytolytic killing of the cancer cells. Recently published preclinical data in an immune competent MM mouse model also show that intravenous RV did not replicate within BM myeloma cells, but instead led to a significant immune reaction [18].

Treatment with PIs (e.g., bortezomib [BTZ], carfilzomib [CFZ]), immunomodulatory drugs (e.g., lenalidomide, pomalidomide), CD38-directed antibodies (e.g., daratumumab and isatuximab), and dexamethasone is currently standard of care for MM patients [19]. One mechanism of action attributed to PIs is the killing of MM cells via inhibition of NF- κ B activation, by blocking the proteasomal degradation of the main NF- κ B inhibitor, I κ B α [20]. Previous data have shown that RV-induced MM cell killing is potentiated by BTZ, either as a direct effect against MM cells by increasing RV-induced endoplasmic reticulum stress [21], or as an immune modulatory effect of the PI, BTZ, when combined with RV in a phase 1b trial [22]. However, the molecular mechanisms behind this observation were not explored. Supporting a possible indirect effect of PI in enhancing viral replication, a recently published paper showed that the addition of BTZ enhances the permissiveness of tumor-associated endothelial cells, leading to enhanced viral delivery to MM cells and thereby stimulating cytokine release [23], but the importance of the immune cells in supporting these mechanisms, independently of the PI sensitivity of the MM cells, has not been explored so far.

Here, using human primary samples and MM animal models, we investigated the mechanisms behind the ability of PIs to enhance the activity of RV (Pelareorep), independently of its direct effect on the cancer cells. We demonstrated that the immune-modulatory activity of PIs positions it as an ideal therapeutic companion to enhance oncolytic viral therapy, even in the presence of PI-resistant MM cells. We also report the results of the first two cohorts of a phase 1b trial of CFZ+Pelareorep along with correlative studies in PI-resistant MM patients

supporting the use of PIs in combination with oncolytic viral therapy.

Methods

Study design

We present clinical and correlative data from NCI 9603, a phase 1b trial testing carfilzomib and Pelareorep, the proprietary form of reovirus, in patients with relapsed MM. Patients with relapsed and refractory myeloma according to the International Myeloma Working Group (IMWG) diagnostic criteria for symptomatic myeloma were enrolled. Patients must have received prior lenalidomide and bortezomib therapy, progressed on or within 60 days of the most recent therapy, and had an Eastern Cooperative Oncology Group (ECOG) performance score ≤ 2 or Karnofsky Performance Status $\geq 60\%$. Prior autologous and allogeneic transplantations were permitted.

Patients were required to have measurable disease defined as serum monoclonal protein ≥ 500 mg/dL, > 200 mg of monoclonal protein in a 24-hour urine sample, or serum immunoglobulin free light chain ≥ 100 mg/L with an abnormal kappa to lambda free light chain ratio. Adequate organ and marrow function was required. There was no serum creatinine requirement. Exclusion criteria included congestive heart failure with a LVEF $< 50\%$ at the time of screening.

The primary objectives were to (1) determine safety and tolerability and define the maximum tolerated dose of the regimen; and (2) obtain evidence of reovirus entry into myeloma cells. Patients were enrolled per a standard 3+3 dose escalation schedule.

Correlative studies are included from patients with relapsed MM who were treated with Pelareorep alone in a previously published phase 1 study [17].

Mice

5-TGM1 murine myeloma cells were harvested during the logarithmic growth phase and injected in 12 immune competent C57BL/KaLwRijHsd mice (0.05 mL/mouse containing 1×10^5 cells in PBS). Cells were injected intraperitoneally, and tumor progression was monitored weekly by mandibular bleeding. CD138⁺ cells were detected by flow cytometry. On day 28, mice were randomized in 2 different treatment groups. One group was treated with a solution of clodronate-liposomes (dichloromethylene diphosphonate-liposome solution) (Encapsula Nanoscience LLC, liposomal clodronate Cat. #NC0337390) to induce monocyte/macrophage depletion and then injected intravenously with 1×10^7 TCID₅₀ of RV, while the second group received only Encapsome (plain liposomes for control) solution before RV injection. Control group mice treated only with plain liposomes solution or clodronate-liposomes alone were also included. After 48 h, mice were euthanized, and femurs were collected.

BM mononuclear cells (BM-MNCs) were isolated and processed by flow cytometry to assess RV capsid formation and confirm the expected macrophage depletion.

Mass cytometry (CyTOF) staining and acquisition

A total of $2-4 \times 10^6$ peripheral blood mononuclear cells (PBMCs) obtained either from MM or healthy donors were stained with a customized panel containing 34 metal-conjugated antibodies (32 surface and 2 intracellular staining and Cell ID cisplatin for non-viable cell detection) (Supplementary Table 4) according to Fluidigm's CyTOF protocols for Cell-ID Cisplatin (PRD018 version 5) (Cat. 201064) and Maxpar Cytoplasmic/Secreted Antigen Staining with Fresh Fix (400279 Rev 05). Non-commercial metal-conjugated IgG1 purified antibodies were purchased from BioLegend (Supplementary Table 5) and in-house conjugated according to Fluidigm's protocol for Maxpar Antibody Labeling (PRD002 Rev 12). PBMCs derived from Reovirus-treated patients (NCI Protocol 9603 IRB 00105298) were stained with Fluidigm's Maxpar Direct Immune Profiling Assay Cell Staining (PN 400286 B1). Samples were acquired, exported as FCS files, and normalized on Fluidigm's Helios (Software 7.0.5189).

CyTOF analysis

Non-custom panel analysis was performed using Maxpar Pathsetter™ software powered by GemStone 2.0.41, Verity Software House, Topsham, Maine. (version 2.0.45). Custom panel FCS files were manually analyzed using FlowJo™ Software (Windows edition, Version 10.6. Becton Dickinson Company; 2019), the Cytobank® platform (<https://www.cytobank.org>) (Cytobank, Inc., Mountain View, CA) for gating and t-SNE plots, and FlowSOM analyses for T cells and monocytes.

T-cell receptor variable beta chain sequencing

Immunosequencing of the CDR3 regions of human TCR β chains was performed using the ImmunoSEQ® Assay (Adaptive Biotechnologies, Seattle, WA). Extracted genomic DNA was amplified in a bias-controlled multiplex PCR, followed by high-throughput sequencing. Sequences were collapsed and filtered to identify and quantitate the absolute abundance of each unique TCR β CDR3 region for further analysis as previously described [24–26]. The fraction of T cells was calculated by normalizing TCR- β template counts to the total amount of DNA usable for TCR sequencing, where the amount of usable DNA was determined by PCR amplification and sequencing of several reference genes that are expected to be present in all nucleated cells.

Statistics

For longitudinal analysis of PB and BM of patients to detect significant differences between pre (C1D1) and

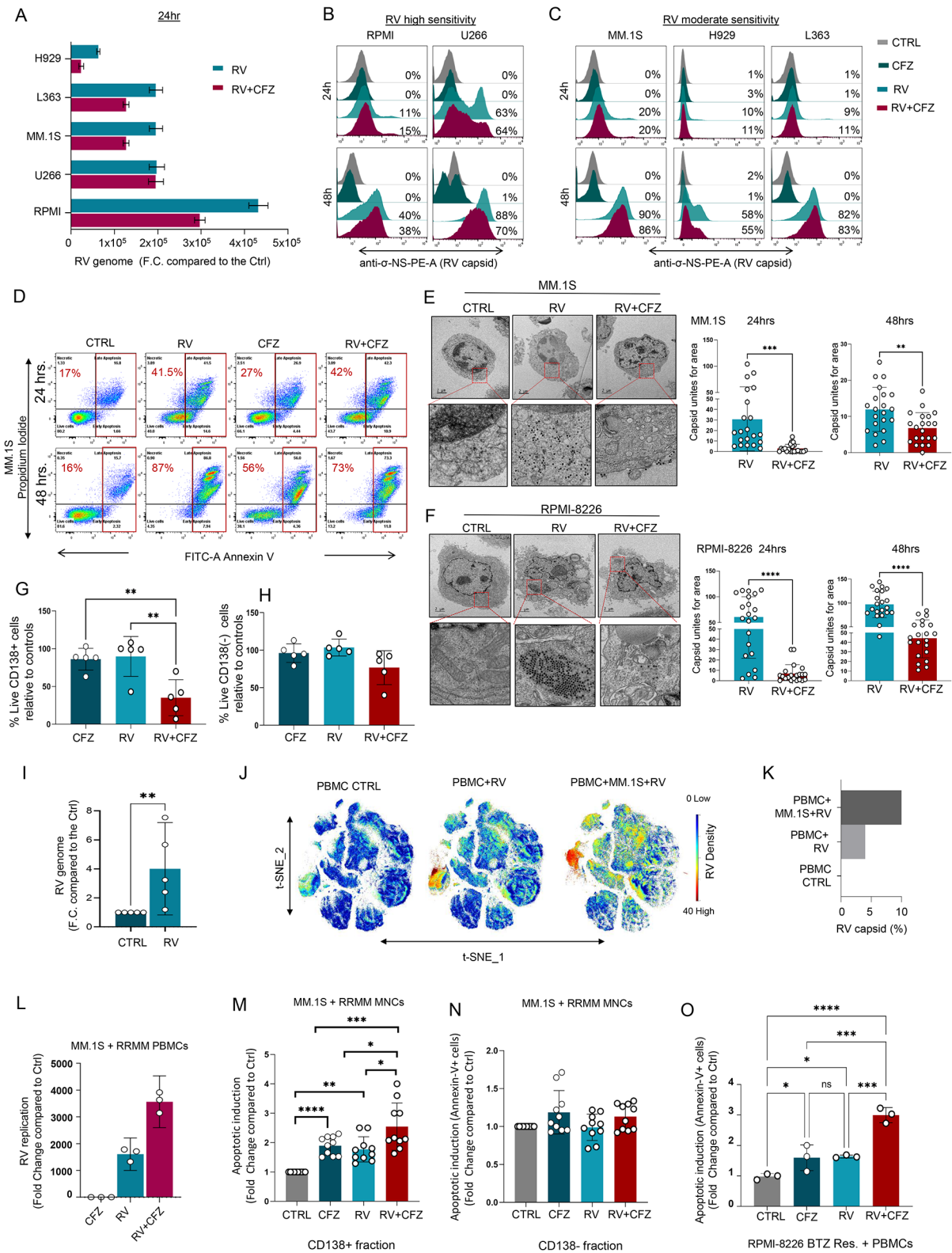


Fig. 1 (See legend on next page.)

(See figure on previous page.)

Fig. 1 PIs potentiate RV-induced MM cell killing only with the involvement of the microenvironment. **(A)** MM cell lines (RPMI-8226, U266, MM.1S, L363, H929) were treated with CFZ (5 nM) and/or Pelareorep (5 MOI) for 24 h to assess the RV genome (mRNA) expression by q-RT-PCR; **(B-C)** Offset histograms showing sigma non-structural capsid protein (σ -NS) on cell lines with high (RPMI-8226, U266) and moderate (MM.1S, H929, L363) sensitivity to Pelareorep infection treated with either CFZ (5 nM) or Pelareorep (5 MOI) as single agent or in combination for 24 and 48 h; **(D)** Representative flow cytometry plots using Annexin V-FITC/PI staining for apoptosis, showing the apoptotic rate (%) of MM.1S cells exposed to both CFZ (2.5 nM) and RV (5 MOI) alone or in combination for 24–48 h; **(E-F)** Transmission electron microscopy (TEM) and related quantification of MM.1S (E) and RPMI-8226 (F) cells treated with CFZ (5 nM) or Pelareorep (5 MOI) alone or in combination for 24 h and 48 h. TEM images were taken at nominal 11,000 x magnification. Statistical analysis was performed using two-tailed unpaired t-test: $***\leq 0.01$ (MM.1S 24 h), $**p\leq 0.01$ (MM.1S 48 h), $****p\leq 0.0001$ (RPMI 24–48 h); **(G)** Bar graph showing significant decrease in cell survival (%) in the CD138+ fraction (MM cells) treated with CFZ + RV compared to the single agents for 48 h, and ordinary one-way ANOVA test was performed $**p\leq 0.01$ in $n=4$ MM patients; **(H)** Bar graph showing no significant decrease in cell viability (%) in the matched CD138neg fraction in the same experimental conditions; **(I)** RV capsid mRNA level expression in healthy donor (HD) PBMCs infected with RV (10 MOI) as fold change (F.C.) compare to the CTRL. Data are expressed as the mean \pm SEM ($n=5$ HDs), normalized compared to control GAPDH; $**p\leq 0.01$; **(J)** A 34-Ab CyTOF panel was used to generate FCS files. Hierarchical clustering and statistical mapping were performed algorithmically via Cytobank© platform. vi-SNE analysis (iterations=4000, perplexity=50) is displayed as 2D plots using the resultant t-SNE_1 and t-SNE_2 dimensions. t-SNE heatmaps according to the density expression of RV capsid (Tb159Di) was gated for the total leukocytes from an HD PBMC infected or not with RV (10 MOI), or in Pelareorep-treated PBMCs to which we added for 1 h MM.1S cells that had been pre-infected for 24 h; **(K)** Bar graph showing RV capsid signal intensity (%) from treatment conditions in (J); **(L)** q-RT-PCR of the viral genome expression of PBMCs isolated from a RRMM patient, treated or not with RV (5 MOI) and CFZ (2.5nM), and co-cultured with MM.1S cells for 12 h. Data are expressed as the mean \pm SEM in triplicates; **(M-N)** Flow cytometry-based killing assay was performed using mono-nuclear cells (BM=3, PB=2) obtained from RRMM patients co-cultured (8:1) with MM.1S GFP + for 24 h and treated or not with RV (5 MOI) and CFZ (2.5 nM) alone or in combination. Bar graphs showing respectively the killing rate of the CD138+ fraction (M) and the CD138neg fraction (N). Data are expressed in fold change compared to the control in $n=5$ RRMM patients each done in two independent duplicate $****p\leq 0.0001$, $***\leq 0.01$, $**p\leq 0.01$, $*p\leq 0.05$; **(O)** Bar graph showing the apoptotic induction of RPMI-8226-BTZ resistant cells co-cultured with HD PBMCs and exposed to RV (5 MOI) and CFZ (5 nM) alone or in combination. Data are expressed in fold change compared to the control each done in independent triplicate $***\leq 0.01$, $**p\leq 0.01$, $*p\leq 0.05$

post treatment (C1D9) measurements, one-sided Wilcoxon signed-rank tests were performed for matched samples. A p -value < 0.05 was considered statistically significant. Data were analyzed using R software (RStudio, version 1.4). For in vitro experiments, data are reported as mean \pm SD of three to four experiments. For ex vivo studies, blood samples were collected from each HD and were split into the number of treatments under comparison. Appropriate t tests (paired or independent samples; two-sided or one-sided), nonparametric tests (Mann-Whitney U test, Wilcoxon signed-rank test) or one-way ANOVA (when indicated) were performed to assess significant differences between two (or more) treatments and/or groups. P -value < 0.05 was considered statistically significant. Animal data were analyzed by ANOVA followed by Tukey's multiple comparison tests for pairwise comparison.

Further Materials and Methods can be found in Supplementary Materials.

Results

PIs potentiate RV-induced MM cell killing only with the involvement of the microenvironment

In line with previously published results from other groups [23], our data show that PIs do not enhance RV viral replication in MM cell lines. Specifically, when MM cell lines with moderate (MM.1S, L363, H929) and high (RPMI-8226, U266) viral tropism [12] were treated with Pelareorep in combination with CFZ, we observed either decreased or unchanged levels of RNA genome (Fig. 1A) and sigma non-structural capsid protein (σ -NS), compared to cells treated with Pelareorep alone (Fig. 1B, C). Similar effects were observed when the PI BTZ was used

(Supp. Figure 1A, B, C). Additionally, our data show that at early time points (24 h) PI treatment did not increase Pelareorep-induced apoptosis in all the MM cell lines we tested (Fig. 1D and Supp. Figure 1D, E). Increased apoptosis in PI+Pelareorep treated cells was also not observed at a later time point of treatment (48 h) (Fig. 1D). Electron microscopy data additionally showed that, in all MM cell lines we tested (MM.1S, RPMI-8226, U266), the addition of a PI decreased capsid formation. A significant decrease in capsid unit count was observed in these cells at both 24 (MM.1S $p=0.0006$; RPMI $p<0.0001$; U266 $p=0.0005$) and 48 h (MM.1S $p=0.003$; RPMI $p<0.0001$; U266 $p<0.0001$) (Fig. 1E-F and Supp. Figure 1F). This PI-induced decrease in virus formation was not observed in PI-insensitive, Pelareorep-sensitive acute myeloid leukemia cells (THP-1) (Supp. Figure 1G), further supporting that viruses prefer to replicate in viable rather than dying cells [27]. We also did not observe significant differences in plaque forming units (PFU) within Pelareorep and CFZ+Pelareorep treated MM cell supernatants collected 96 h after treatment (Supp. Figure 1H, I).

We then investigated whether PIs could instead increase Pelareorep-induced killing of MM cells in the presence of the tumor microenvironment, independently of its direct anti-MM activity, in both an animal model, as recently published [23], and in the ex vivo setting. Total MM BM-MNCs, which contain CD138+MM cells, fibroblasts, and immune cells, were obtained from patients with MM at different disease stages ($n=5$, 2 smoldering, 1 newly diagnosed and 2 relapsed MM) and treated for 48 h with CFZ or Pelareorep alone or in combination. Our data show a significant decrease in the viable CD138+ fraction (MM cells) treated with PI+Pelareorep,

compared to the single agents (PI+RV versus RV $p=0.01$; PI+RV versus CFZ $p=0.008$) (Fig. 1G), an effect that was not observed in the matched CD138(-) cells in the same experimental conditions (Fig. 1H). MM adhesion to the BM stromal cells displayed resistance to RV infection and induced oncolysis (Supp. Figure 2A), excluding that these cells may contribute to the enhancement of RV-induced MM cell killing activity by PIs. Because it has been reported that, despite the presence of neutralizing antibodies, replication-competent RV can be recovered from PBMCs but not plasma obtained from colorectal cancer patients treated intravenously with a single dose of RV [28], we decided to investigate whether the immune environment would instead be responsible for supporting RV replication and subsequent MM cell infection. When human PBMCs isolated either from patients with MM or healthy donors (HDs) were treated with Pelareorep for 24 h, a significant increase in the viral genome ($p=0.008$, $n=5$ donors) was observed (Fig. 1I), supporting that a limited viral replication can be detected even in non-cancer cells. Consistent with these data, single-cell mass cytometry (CyTOF) analysis showed a localized expression of the inner viral capsid protein σ -NS, whose expression is associated with active viral replication [12, 29], in PBMCs treated ex vivo with Pelareorep for 24 h (Fig. 1J-K and Supp. Figure 2B). A greater increase in capsid expression in human PBMCs was found when MM.1S cells were added to Pelareorep-treated PBMCs (Fig. 1J-K and Supp. Figure 2B), and the capsid signal increased with increased number of virions (Supp. Figure 2C), supporting the specificity of intracellular capsid detection.

These findings prompted us to investigate whether PIs could indeed increase viral replication in the presence of immune cells. Our data show that after 24 h of treatment, the addition of CFZ significantly increased RV replication not only in healthy PBMCs ($p<0.001$) (Supp. Figure 2D) co-cultured with MM cells but also when PBMCs obtained from patients with refractory MM ($n=3$, $p<0.01$) were used (Fig. 1L). Pelareorep-induced MM killing was also enhanced in the presence of CFZ when MM cells (GFP+MM.1S) previously unexposed to the virus were co-cultured either with MNCs from patients with multi-relapsing MM ($n=5$) or healthy donors ($n=3$), at the ratio 8 MNCs:1 MM.1S GFP+cells, compared with effects from each single agent alone (Fig. 1M-N and Supp. Figure 2E).

To assess whether the enhanced CFZ+RV MM cell killing that was observed when MM cells were co-cultured with MNCs was independent of bortezomib (BTZ) mechanisms of resistance, we tested whether this effect was also reproducible in PI-resistant cells (RPMI-8226-BTZ-res). Although, as expected, BTZ-res cells remained insensitive to BTZ treatment compared to the parental cells (WT), both cell lines were equally sensitive to

RV infection (Supp. Figure 2F-G-H). Interestingly, the addition of PBMCs increased BTZ sensitivity in both BTZ-res and WT cells (Supp. Figure 2I). A significant increase in MM cell killing was also observed when BTZ-res cells were co-cultured with PBMCs and treated with CFZ+Pelareorep, compared to levels from each agent alone ($p<0.01$) (Fig. 1O).

Proteasome inhibitor-enhanced viral replication requires monocytes

Because our data suggested that PIs (CFZ and BTZ) improve RV productive infection in PBMCs and subsequent infection and killing of cancer cells, we investigated which immune compartment is responsible for this effect.

Twenty-two different immune compartments including CD4+ and CD8+ T cell subsets (naïve, central memory [CM], effector memory [EM] and terminally differentiated [TEMRA]), natural killer T cells (NKT), classical phagocytic and non-classical monocytes, and NK cells (Supp. Table 1) were interrogated for the presence of viral capsid protein (σ -NS) using CyTOF. After 24 h of Pelareorep treatment, the RV capsid was mainly found in the monocyte compartment (CD45+CD20-CD3-CD56-CD14+HLA-DR+) (Supp. Figure 3A-C). Significant capsid accumulation in the CD14+ fraction, compared to the matched CD14(-) fraction, was observed in all PBMCs isolated from patients with MM ($p=0.034$, $n=3$) and healthy donors ($p=0.03$, $n=4$) (Fig. 2A-C and Supp. Figure 3A-E). Cell cluster visualization self-organizing map (FlowSOM) (Fig. 2B and Supp. Figure 3B) and t-distributed stochastic neighbor embedding (t-SNE) heatmaps (Fig. 2C and Supp. Figure 3C) showed that the σ -NS signal (red) was primarily observed in the Classical monocytes (phagocytic) in PBMCs from both healthy donors and patients with MM. Specifically, we found active viral replication at 24 h in 10% +/- 3.05% of the phagocytic monocytes, but almost no replication was observed in both Intermediate and Non-Classical monocytes (Fig. 2D, E).

We then investigated whether PIs could increase RV in the monocytic fraction. When PBMCs were treated with Pelareorep alone or in combination with CFZ, viral replication occurred exclusively in the Classical monocyte population, with more replication evident following combination treatment (absolute count: 4605 and 4702 [CFZ pretreatment or CFZ+RV co-treatment, respectively] vs. 2890 [RV alone]) as shown by FlowSOM, t-SNE heatmap graphical representation, and heatmap of monocyte compartments from CyTOF of PBMCs from relapsed MM (Fig. 2D-E) and healthy PBMCs (Supp. Figure 3E-G). Analysis conducted in primary CD14+ selected populations by flow cytometry, Western blot, and qRT-PCR confirmed that the addition of PI to RV-infected

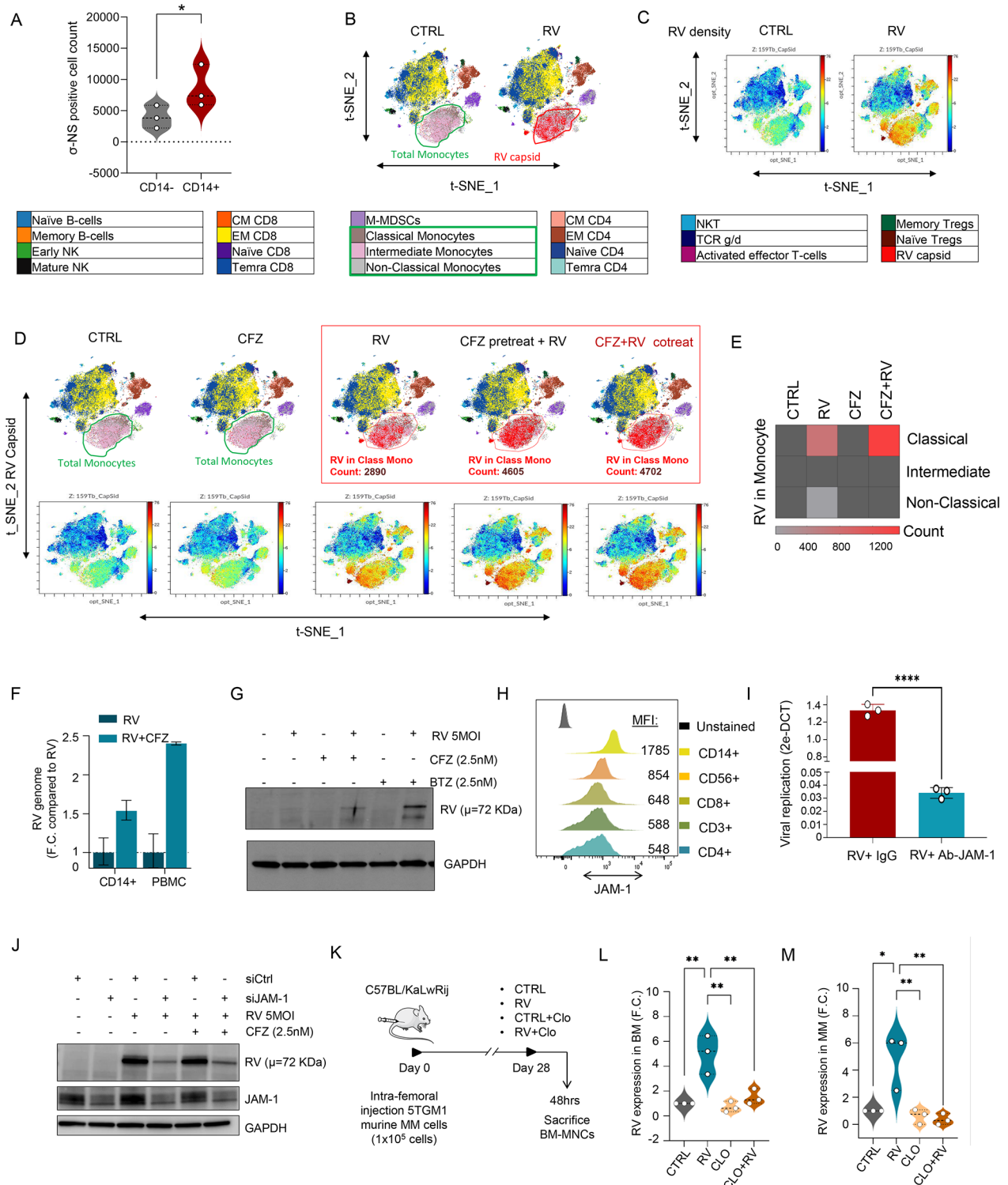


Fig. 2 (See legend on next page.)

cells enhanced capsid formation and replication (Fig. 2E, G and Supp. Figure 3H) based on detection of σ -NS. An increase in RV genome replication upon CFZ treatment was not noted in all major CD14-negative immune

subsets including purified B, T, and NK cells (Supp. Figure 3I).

Because we found active viral replication in the CD14+ fraction, we tested whether the junctional

(See figure on previous page.)

Fig. 2 Proteasome inhibitor enhanced viral replication requires monocytes. **(A)** Violin-plot showing (σ -NS) signal in 3 MM patients analyzed by CyTOF $*p \leq 0.05$; **(B-C)** 34-Ab CyTOF panel used to generate FCS files. Hierarchical clustering and statistical mapping performed algorithmically via the CytoBank platform. vi-SNE analysis (iterations = 3000, perplexity = 100) displayed in 2D plots using the resultant t-SNE 1 and t-SNE 2 dimensions. High-fidelity FlowSOM ("self-organizing map") (metacluster = 10 and cluster = 100) based on vi-SNE 2D plots showing 22 different immune-compartments in total PBMCs of MM patients infected or not with RV (10 MOI). Red signal shows RV capsid (σ -NS) in monocytes **(B)**. t-SNE heatmap highlighting density expression of selected RV capsid (σ -NS) signal **(C)**; **(D-E)** CyTOF high-fidelity FlowSOM in MM-PBMCs infected or not with RV (10 MOI) alone or in combination with CFZ (2.5 nM) and t-SNE heatmap, showing increased RV capsid (σ -NS) detection in Classical Monocytes after RV + CFZ co-treatment or RV + CFZ pretreatment (count: RV = 2890, RV + CFZ pretreatment = 4605, RV + CFZ cotreatment = 4702) **(D)**, and heatmap graphical representation of RV absolute count detection in the different monocyte subsets **(E)**; For each experimental condition the same number of events were acquired and analyzed. **(F)** q-RT-PCR for the viral genome expression of RV-infected HD-PBMCs or isolated HD-CD14+ population after 24 h, normalized to control GAPDH and expressed as the mean \pm SEM of triplicates in fold change (FC) compared to RV alone; **(G)** Western blot analysis of (σ -NS) viral protein in HD CD14+ selected population after 8hrs of PIs (CFZ and BTZ, 2.5 nM) and RV treatments alone or in combination; **(H)** Offset histograms showing JAM-1 flow cytometry detection in different immune subsets as indicated. The experiment was repeated in $n = 3$ independent triplicate; **(I)** CD14+ cells were seeded and incubated with JAM-1 blocking Ab (10-50-100-150 μ g/mL) for 1 h, then infected with RV 5 MOI for 24 h. q-RT-PCR for the viral genome expression was normalized to control GAPDH and expressed as the mean \pm SEM of triplicates compared to RV alone $****p \leq 0.0001$; **(J)** Western blot analysis on THP-1 showing RV (σ -NS) protein detection after specific JAM-1 knockdown; **(K)** Schematic representation of mice experiment: 12 immune competent myeloma mice (C57BL/KaLwRij) were injected intra-femoral with 1×10^5 5TGM1 murine MM cells and treated with 150 mg/kg clodronate-liposome for monocytes-macrophages depletion or control, then with or without intravenous injection of RV (5×10^8 TCID₅₀) for 48 h; **(L-M)** Violin plots showing bone marrow RV (σ -NS) capsid formation ($**p \leq 0.01$) **(L)** of treated mice and in MM-CD138+ cells ($**p \leq 0.01$ and $*p \leq 0.05$) **(M)**, analyzed by flow cytometry

adhesion molecule 1 (JAM-1) receptor [9] mediates RV entry in this cellular subset. Flow cytometry analysis of different immune cell subsets in healthy donor PBMCs revealed high JAM-1 expression on the surface of the monocyte population (Fig. 2H and Supp. Figure 3J). When primary CD14+ cells were pre-treated with an anti-JAM-1 blocking antibody, we observed that RV replication was significantly downregulated (Fig. 2I). Moreover, following knockdown of JAM-1 expression in a monocytic-like cell line (THP-1), viral replication was also strongly impaired as shown by Western blot analysis (Fig. 2J and Supp. Figure 3K, L).

To assess whether the CD14+ fraction is critical for RV delivery to the cancer cells in vivo, we induced monocyte/macrophage depletion in an immunocompetent MM animal model using clodronate liposomes (Clo). Specifically, 1×10^5 murine MM 5-TGM1 cells were intra-femorally injected into syngeneic C57BL/KaLwRij mice. After 28 days, mice were randomized to receive clodronate liposomes (Clo) plus RV (1×10^7 termination of the 50% tissue culture infectious dose [TCID₅₀]) or control liposomes (CTRL) plus RV (1×10^7 TCID₅₀). Mice treated with only Clo or CTRL were also included as internal controls (Fig. 2K). After 48 h, RV capsid formation by flow cytometry in BM-MNCs and in MM-CD138+ cells was significantly lower in the Clo+RV treated group compared to that in the CTRL+RV group ($p = 0.004$) (Fig. 2L, M and Supp. Figure 3M).

CFZ impairs the monocyte-mediated antiviral response without affecting T cell activation

Oncolytic viruses induce an antiviral immune response [30] that is often accompanied by nuclear factor kappa B (NF- κ B) activation [31] and dysregulated release of inflammatory cytokines from monocytes to block active viral infection [32]. For this reason, we investigated whether Pelareorep could induce NF- κ B activation in

monocytes. Immunofluorescence analysis at both 2 and 4 h after RV infection of a monocytic cell line (THP-1) showed a significant increase in p65 nuclear translocation compared to that in the RV-untreated cells ($p < 0.0001$) (Supp. Figure 4A, B), an effect that was similar to one observed in cells treated with the specific NF- κ B activator TNF- α (Supp. Figure 4A-C). A significant decrease in p65 nuclear translocation was observed when CFZ was added to RV-treated cells ($p < 0.0001$), supporting that PI impairs NF- κ B activation upon RV infection. (Supp. Figure 4C). A significant decrease ($p = 0.0001$) in p65 nuclear translocation was also observed when CFZ was added to RV-treated primary CD14+ monocytes isolated either from healthy or relapsed/refractory MM (RRMM) donors in the same experimental conditions (Fig. 3A-C), supporting that this phenomenon is general.

Since our data suggested that CFZ increases RV productive infection in circulating monocytic cells, we investigated whether blocking NF- κ B activation could impair the expression of the anti-viral IFN-I response. Our data show that RV infection of PBMCs increased IFN- α and IFN- β expression, an effect that was reverted by the addition of the NF- κ B specific inhibitor Bay-11 (Fig. 3D, E). Aligned with this observation, our data show that, when MM.1S cells were co-cultured with PBMCs from RRMM donors, the addition of Bay-11 also potentiated the anti-MM activity of RV (Fig. 3E, G). This effect was associated with enhanced capsid formation (Fig. 3H), as also shown by Western blot analysis in a monocytic cell line (Fig. 3I). An NF- κ B reporter luciferase assay also showed that the addition of CFZ decreased NF- κ B transcriptional activation, which was induced upon RV infection (Fig. 3J).

As expected, IFN- α and IFN- β expression were also significantly impaired in CFZ+RV treated cells compared to RV alone at different timepoints (Fig. 3K, L and Supp. Figure 4D-G), an effect that was observed exclusively in

the monocytic fraction (CD14+ population) (Supp. Figure 4H, I).

A cytokine array analysis conducted in the CD14+ fraction isolated from either healthy donors or patients with relapsed MM showed that RV-treated PBMCs for 4 h released pro-inflammatory cytokines (IL-8, IL-10, IL-12, IL-13, and TNF- α) and chemokines (MIP-1 α and β , MIG, IL-8, MCP-1) (Fig. 3M and Supp. Figure 4J), an effect that was almost completely abrogated by adding a PI (CFZ or BTZ) or Bay-11 (Fig. 3M and Supp. Figure 4J). q-RT-PCR analysis also confirmed that the addition of BTZ arrested IFN- α and IFN- β expression (Supp. Figure 4K).

In-depth clustering CyTOF analysis revealed that RV infection induced significant upregulation of the early activation marker CD69 in the monocytes and T cells and of the T cell costimulatory receptor CD80 in the monocytic fraction of freshly isolated PBMCs obtained from either patients who were treated with dexamethasone and PI-based regimens or healthy donors (Fig. 3N, O and Supp. Figure 4L, M). Addition of CFZ to RV did not significantly decrease the expression of CD69 or CD80, in the monocytic or T cell fraction isolated from patients with relapsed MM or in healthy donors (Fig. 3O, P and Supp. Figure 4M). The increase in T cell co-stimulatory molecules in the monocytic fraction is aligned with recently reported murine data in which T cell activation occurred in immune competent mice treated with RV alone or RV combined with a PI [23]. Because polarized monocytes, in addition to inducing T cell responses, can also act as scavenger cells, we tested whether, besides promoting virus delivery to MM cells, CFZ could also potentiate monocyte phagocytosis. For this purpose, we isolated CD14+ fractions from the PBMCs obtained from one patient; the phagocytic activity of the monocytes after polarization was detected by live cell-imaging microscopy. Our data show that CFZ treatment induced a significant increase in phagocytic activity of polarized monocytes (Fig. 3Q, R).

Because we were limited by the number of isolated CD14+ cells, phagocytic activity of MM cells upon CFZ treatment was instead assessed in healthy donor PBMCs using flow cytometry-based analysis. After an overnight incubation, CD14+ populations from each treatment group were purified and co-cultured with GFP+MM cells (MM.1S) for 24 h. We observed significant increase in phagocytic activity when CD14+ cells were pre-treated with both PI and RV compared to control saline treated CD14+ cells ($p=0.018$), as shown by the surge of a double positive (CD14+/GFP+) cellular population (Fig. 3S, T). Significantly higher MM cell death was also observed when the CD14+ fraction was pre-treated with RV+CFZ, compared to each single agent, using the same experimental settings associated with an increase in RV productive infection (Supp. Figure 4N, O).

RV combined with CFZ increases viral replication in the bone marrow of patients with MM

We previously showed in a phase 1 trial that replicating viral genome is found in the MM cells of relapsed patients treated with single agent Pelareorep, but neither active RV replication, as defined by concomitant robust viral capsid production, nor significant clinical response [17] was observed. Because our preclinical data showed that PI increased infection of monocytes and subsequent delivery of virus to the MM cells, we tested this concept in specimens obtained as part of a phase 1b study of RV in combination with CFZ in relapsed myeloma (NCT02101944). Patients were treated on days 1, 2, 8, 9, 15 and 16 of a 28-day cycle. Pre-treatment samples (baseline) were collected just prior to cycle 1 day 1 RV+CFZ infusion for each patient. Treatment included intravenous dexamethasone followed by intravenous CFZ for over 30 min, and then RV infusion over 60 min. We aimed to identify the maximum tolerated dose of Pelareorep combined with CFZ. All safety analyses were conducted during cycle 1. Patients were infused with CFZ 20 mg/m² on days 1 and 2 of cycle 1, and 27 mg/m² thereafter. The starting dose of Pelareorep was 3×10^{10} TCID₅₀/day, and all patients received dexamethasone 20 mg on each treatment day (Fig. 4A).

Thirteen patients were enrolled; baseline demographics are summarized in Supplementary Table 2. All patients were Caucasian, seven were male, six were female, and the median age was 60 (range 43–70). The median International Staging System stage at diagnosis was 2 (range 1–3), and one patient was dialysis dependent. Six patients had evidence of high-risk cytogenetics (+1q21, t(4;14), t(14;16) or del17p) at the time of diagnosis, and ten had high-risk cytogenetic features at the time of screening. The median number of prior therapies was 4 (range 2–12), and prior lines of treatment was 2.5 (range 1–9). All patients were lenalidomide refractory and BTZ exposed, 84.6% (11/13) were BTZ refractory, two patients were pomalidomide refractory, and one patient was CD38 antibody refractory. Five patients were CFZ exposed, and all were considered to be refractory (Supp. Table 3); 3 of these patients had evidence of disease progression during CFZ treatment, while two others were deemed carfilzomib refractory based on lack of achieving response while on treatment [33]. All patients previously CFZ exposed were treated per historical standard of care dosing including treatment on days 1, 2, 8, 9, 15, and 16 of 28-day cycles (20 mg/m² on cycle 1 days 1 and 2, followed by 27 mg/m² thereafter), and three patients had received two prior CFZ-containing regimens. The median duration of exposure to CFZ in these five patients was 8 months (range 1.5–20), and the best overall response to a CFZ-containing regimen in these patients was a partial response.

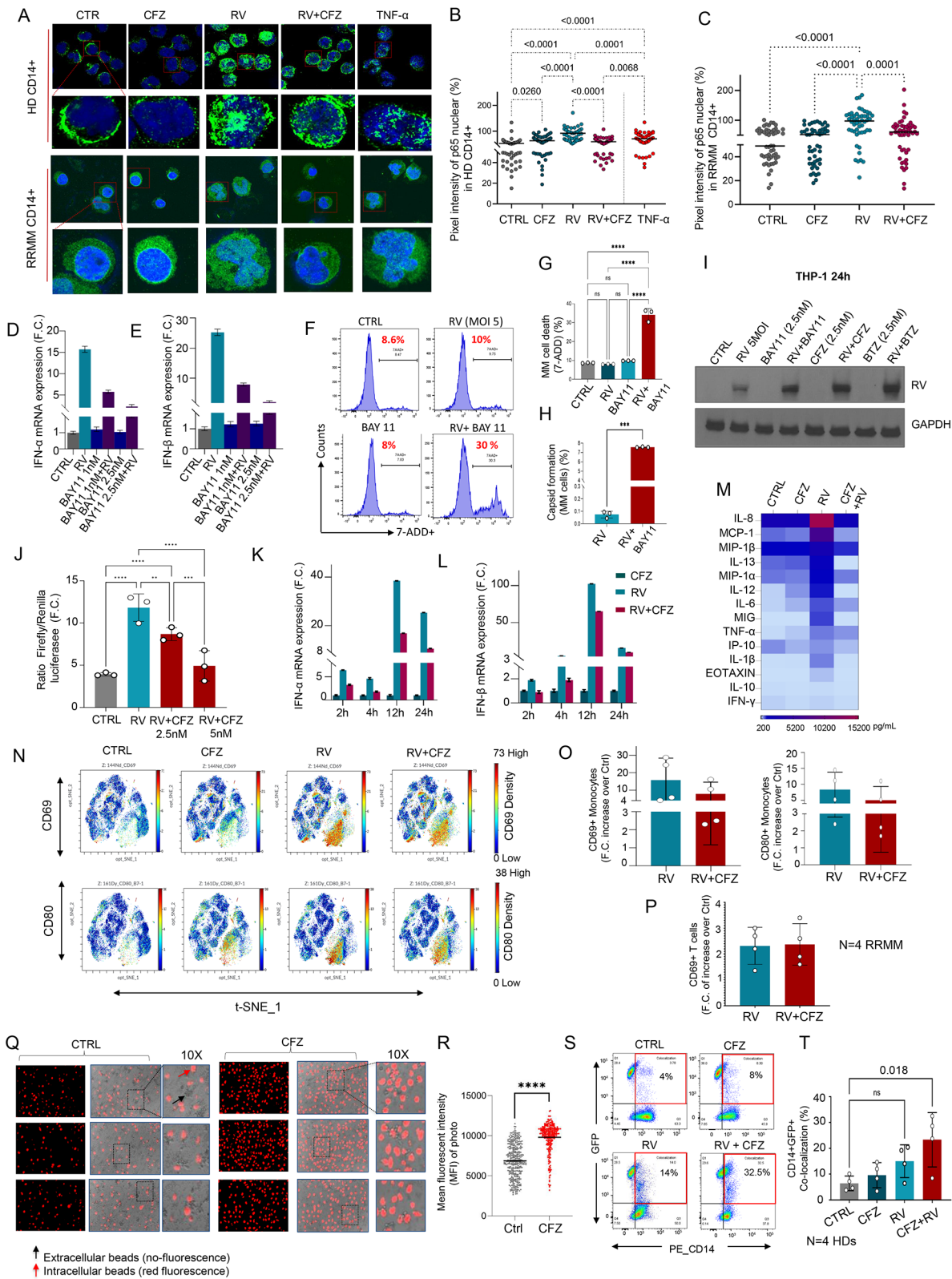


Fig. 3 (See legend on next page.)

(See figure on previous page.)

Fig. 3 CFZ impairs the monocyte-mediated antiviral response without affecting T cell activation. **(A)** Representative merge of immunofluorescence fields showing p65 staining (green) as indicated and DAPI staining for nucleic acids (blue) in HD and RMM CD14+ isolated cells treated with CFZ for 30 min, then infected or not with RV (5 MOI) for 2–4 h. TNF- α (50 ng/ml) was used as a positive internal control showing p65 nuclear translocation; **(B–C)** Imaging-based quantification up to 2 h of fluorescence staining intensity vs. pixel position of 50 representative cells in HD (B) and 4 h for RMM CD14+ isolated cells (C). Comparisons among groups were performed by one-way ANOVA: $***\leq 0.01$, $****p\leq 0.0001$; **(D–E)** Histograms showing IFN- α (D) and IFN- β (E) mRNA expression of RV infected (5 MOI) or uninfected HD-PBMCs and treated with different concentrations (1 or 2.5 nM) of Bay-11 for 24 h and normalized to control GAPDH. Data represent the mean \pm SD expressed in F.C. compared to the control; **(F)** Flow cytometry-based killing assay was performed using HD PBMCs co-cultured (8:1) with MM.1S GFP+ for 24 h and treated or not with RV (5 MOI) and Bay-11 (2.5 nM) alone or in combination; the experiment was repeated in $n=3$ independent replicates **(G)** Bar graph showing the killing rate as 7-AAD in % expressed as the mean \pm SEM of triplicates $****p\leq 0.0001$; **(H)** q-RT-PCR showing RV capsid formation in the same experimental conditions used in F. Data are normalized and expressed as mean \pm SD in F.C. compared to the control GAPDH; **(I)** Western blot assay on THP-1 cells showing RV (σ -NS) protein detection after treatment with Bay-11, BTZ, CFZ 2.5 nM and RV 5 MOI alone or in combination; **(J)** Luciferase reporter assays in HEK293 cells transfected with plasmids encoding a NF- κ B luciferase reporter gene, and treated with RV (5MOI) and CFZ (10 nM and 2.5 nM) up to 72 h; TNF- α (5 ng/ml) was added to all the wells. NF- κ B activity was determined by luciferase assay (mean \pm SD ($n=3$), $****p\leq 0.0001$, $***\leq 0.01$, $**p\leq 0.01$); **(K–L)** q-RT-PCR showing IFNs type I (IFN- α and IFN- β) induction after RV (5 MOI) and CFZ (2.5 nM) treatments in HD PBMCs at different time points (2–4–12–24 h). Data are normalized to control GAPDH and expressed as mean \pm SD in F.C. compared to the control; **(M)** Heatmap of multiplex cytokine profile performed on supernatant from PBMCs from an HD treated for 4 h with CFZ, RV or both, showing 14 out of 22 of the analyzed cytokines, in which the signal was detected; **(N–O–P)** Mass cytometry t-SNE heatmaps showing CD69 and CD80 expression in RMM isolated PBMCs with or without RV infection (10 MOI) and CFZ treatment (2.5 nM) for 24 h; Bar graphs showing CD69 and CD80 relative expression in the monocytes (O) and CD69 in the T cells (P) of $n=4$ RMM patients. Data are expressed as mean \pm SD in F.C. compared to the control; **(Q–R)** Three representative fields for each treatment conditions of live-cell imaging of phagocytic activity of CD14+ cells isolated from one patient showing higher phagocytic ability of CFZ-treated macrophages compared to the control macrophages as shown by the significant difference in the mean fluorescence intensity (MFI) (right) (R); **(S–T)** Representative flow cytometry analysis showing the gating strategy for one out of $n=4$ different healthy donors analyzed and dot plot (S) showing increased CD14+ co-localization with MM.1S GFP+ cells after overnight incubation with RV (5 MOI) + CFZ (2.5nM) treatments. Data analyzed by one-way ANOVA

The ten most common treatment-emergent toxicities per CTCAE v5.0 in cycle 1 included hypertension (one grade 2 and four grade 1), thrombocytopenia (two grade 3, one grade 2, one grade 1), anemia (one grade 2 and 3 grade 1), dyspnea on exertion (one grade 2, three grade 1), myalgia (three grade 1), fever (one grade 2, one grade 1), lymphopenia (one grade 3 and one grade 1), nausea (one grade 2, one grade 1), and diarrhea (one grade 1, one grade 2) (Supp. Figure 5A). Two patients (ID 2 and ID 5) experienced dose-limiting toxicities, specifically thrombocytopenia (with bleeding) and acute congestive heart failure, attributable to CFZ and possibly related to Pelareorep, respectively. Because of these toxicities, subsequent patients were treated at dose level –1 with CFZ 20 mg/m² and Pelareorep 3 \times 10⁹ TCID₅₀/day on all treatment days.

Eleven patients completed at least one cycle of treatment and were evaluable for response. The response outcomes from baseline include very good partial response (VGPR, $n=2$), partial response (PR, $n=4$), minor response (MR, $n=1$), stable disease (SD, $n=3$), and progressive disease in one patient (Fig. 4B, and Supp. Figure 5B). The two patients who experienced a DLT following two doses of combination treatment had a 96% (patient ID 2) and 27% (patient ID 5) reduction in measurable disease, respectively.

In those patients with BTZ-refractory disease, responses included VGPR ($n=2$), PR ($n=4$), and SD ($n=3$). Responses in patients previously treated with CFZ included PR ($n=1$), MR ($n=1$), and SD ($n=3$). Including all patients evaluable for response, those treated at dose level 1 (DL1) had deeper responses than those treated

at dose level –1 and remained on treatment for a longer period of time (mean days of treatment 331.6 [range 84–576] vs. 54.5 [range 28–84], respectively), findings that suggest a dose-dependent effect (Fig. 4B). BM aspirates of each patient enrolled in both single agent RV and CFZ+RV trials were collected at baseline and after a week of treatment to assess RV infection (viral genome) and replication (viral capsid) in the BM of treated patients. While active RV productive infection was not observed in our previously reported trial of single-agent RV [17], as clearly shown by the presence of increased intracellular viral genome but with minimal capsid protein (Fig. 4C and Supp. Figure 5C), in the CFZ+RV treated patients, both RV genome and capsid were found indicative of productive reoviral infection (Fig. 4D and Supp. Figure 5D). Our data showed increased capsid expression in the BM of patients treated with a low dose CFZ (DL-1) compared to baseline ($p=0.004$), and this effect was further potentiated in patients treated with a standard dose of CFZ (DL1) ($p=0.028$) (Fig. 4E). Consistent with the preclinical data of Kelly et al. [21], we also found a significant upregulation of the checkpoint inhibitor PD-L1 in five post treatment BM biopsies obtained from patients treated with RV+CFZ ($p=0.005$), compared to the baseline at pre-treatment (Fig. 4F–G–H and Supp. Figure 5E, F). This upregulation was not observed in the biopsies obtained from our trial of RV monotherapy (Fig. 4H). Significant caspase-3 activation was also found in tumor biopsies of patients treated with RV+CFZ, compared to the baseline levels ($p=0.005$, $n=5$) (Fig. 4I). Caspase-3 activation was not found in the available longitudinal

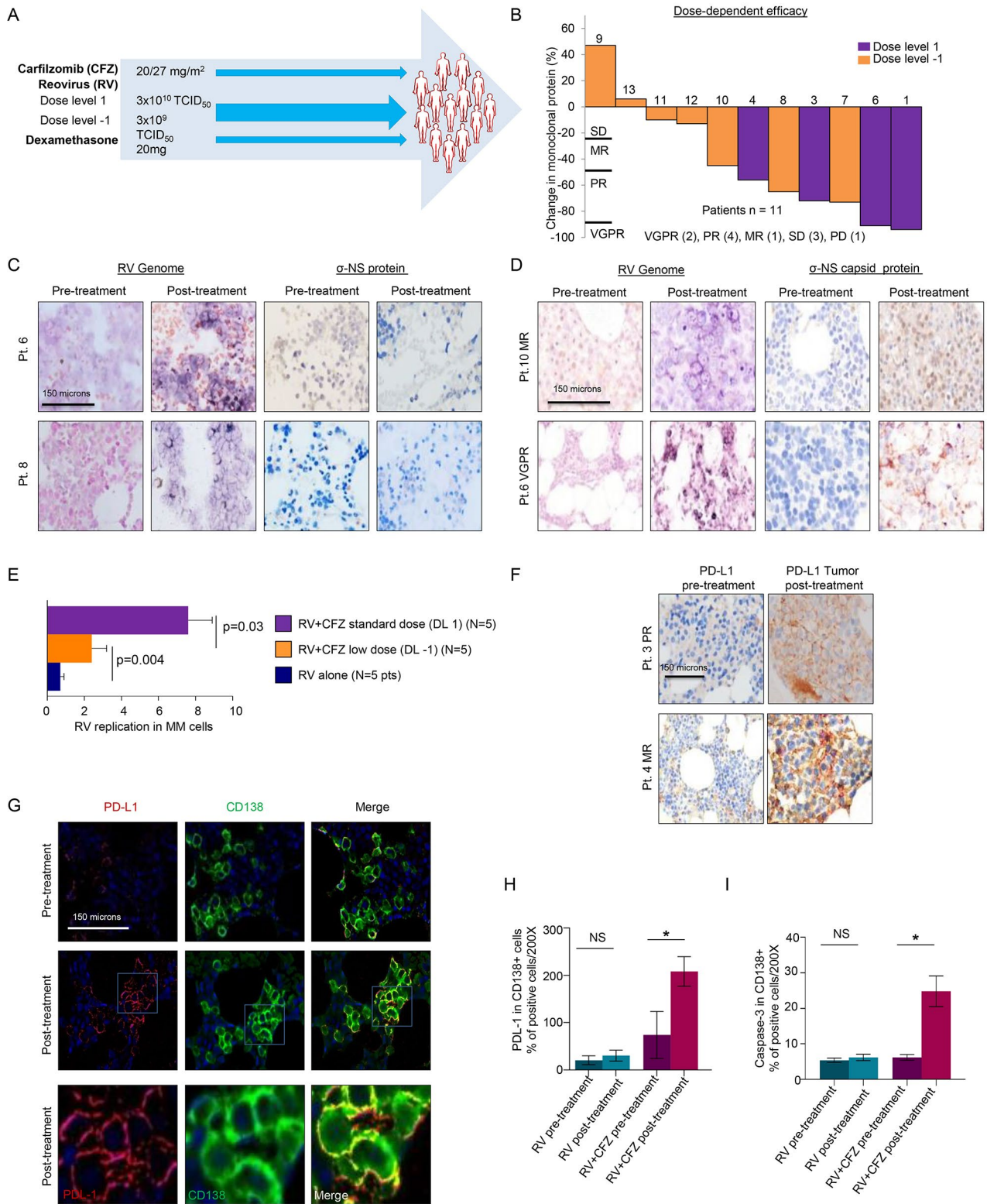


Fig. 4 (See legend on next page.)

(See figure on previous page.)

Fig. 4 RV combined with CFZ increases viral replication in the bone marrow of MM patients. **(A)** Schematic representation of the treatment schedule for patients with relapsed MM enrolled in Phase 1b clinical trial of the combination of Pelareorep and carfilzomib; **(B)** Waterfall plot illustrating best response of each patient. The overall response rate (ORR) was 53.8% (7/13) and clinical benefit rate (CBR) was 69.2% (9/13). Patients treated at dose level 1 had an overall response rate (ORR) of 83.3% (5/6) and clinical benefit rate (CBR) of 100%. Responses at this dose level included very good partial response (VGPR, $n=2$), partial response (PR, $n=4$), minimal response (MR, $n=1$) stable disease (SD $n=3$), and progressive disease (PD $n=1$). Patients treated at dose level -1 had an ORR of 28.6% (2/7) and CBR of 42.9% (3/7); **(C-D)** 4X magnification images of immunohistochemistry (IHC) showing the in-situ data for the detection of reoviral RNA (signal blue with pink counterstain) and reoviral capsid protein (signal brown with blue counterstain) pre and post-treatment in RV alone and RV+CFZ treated patients. Note that reoviral RNA is evident only after post-treatment and that many more cells have detectable viral RNA compared to the capsid protein in the serial sections; **(E)** Bar graph showing α -NS protein detection at a low and standard dose of CFZ ($p=0.028$) in the BM. Each value represents the number of positive cells per 200x field; **(F)** 4X magnification images of IHC of PD-L1 protein (signal brown with blue counterstain) pre and post-treatment ($n=5$); **(G)** 4X magnification images of immunofluorescence showing the co-expression of PD-L1 (fluorescent red) and CD138 (fluorescent green), and 20X magnification at post-treatment Merged image with co-expression seen as fluorescent yellow (scale bars at 150 micrometers); **(H-I)** Bar graph showing significant upregulation of PD-L1 (H) and Caspase-3 on the surface of MM cells (I) ($p=0.005$) in RV+CFZ treated patients relative to pre-treatment ($n=5$) an effect was not observed in the RV only treated pts. Each value represents the number of positive cells per 200x field

biopsies of patients treated with RV alone ($n=5$), further supporting the lack of active viral replication.

RV combined with PI induces immune activation

To assess whether RV combined with PI treatment could induce changes in the monocytic and T cell compartments of patients with MM, as we observed in ex vivo studies, we performed longitudinal flow cytometry analysis of the peripheral blood (PB) obtained from RV+CFZ treated patients collected at pre-treatment (immediately before C1D1) and during treatment (C1D2-9-15-22-28; C2D1; C3D1). In the first week of treatment, we observed a significant increase in the number of overall monocytes ($p=0.006$) (Fig. 5A and B), an increase that was mainly due to the expansion of the Classical phagocytic monocyte compartment ($CD14^{++}CD16^{-}$) ($p=0.03$) (Fig. 5C). Aligned with our preclinical data, a significant increase in activated monocytes ($CD69^{+}$) was also observed ($p=0.047$) (Fig. 5D, Supp. Figure 6A). No significant differences were observed in total and activated monocyte levels between CFZ-exposed and naïve patients enrolled in the trial. Although, when analyzed separately a significant increase in $CD69^{+}$ monocytes compared to baseline was only observed in CFZ-naïve, but not in CFZ exposed patients, in which upregulation was observed only in two out of 4 patients (Fig. 5E). Analysis of the T cell compartment revealed a strong increase of $CD8^{+}$ T cell frequency upon treatment, especially up to C1D9 ($p=0.04$) (Fig. 5F and Supp. Figure 6B) and correlated with a substantial reduction of $CD4^{+}$ cells ($p=0.03$) (Fig. 5G and Supp. Figure 6C), as well as a significant reduction upon treatment of the $CD4/CD8$ ratio ($p=0.04$) (Fig. 5H and Supp. Fig. 5D). Consistent with these data, we found increased expression in the cell cycle marker Ki-67 in total blood lymphocyte T cells upon treatment (C1D9), compared to baseline levels (C1D1) ($p=0.004$) (Supp. Figure 6E, F), which paralleled Ki-67 expression in the $CD8^{+}$ T cell population (Supp. Figure 6G). Longitudinal CyTOF analysis in 1 CFZ-resistant (RRMM-1) and two BTZ resistant (RRMM2, RRMM3) patients indicated monocyte

increase, as shown by FlowSOM cell cluster visualization of the different immune populations (Fig. 5I). Specifically, high-dimensional t-SNE heatmaps confirmed increases in the $CD14^{+}$ monocytic fraction in all three MM patients analyzed by CyTOF (Fig. 5J-L). Subcluster characterization indicated a specific increase in classical phagocytic monocytes (Fig. 5M-O). The total count of circulating regulatory T cells (Tregs) was sharply reduced after the first cycle of therapy in all analyzed samples from patients with MM (Fig. 5P-R). Moreover, an in-depth classification of this population showed the same trend in both memory and naïve Tregs (Fig. 5P-R). Collectively, our data indicate a robust immune activation in Pelareorep+CFZ-treated patients.

RV combined with CFZ treatment promotes T cell responses against MM cells

Because we observed an increase in cytotoxic $CD8^{+}$ T cells after monocytic expansion, we then investigated whether T cell proliferation induced by RV+CFZ could also be associated with changes in T cell clonality. Therefore, we analyzed the T cell receptor (TCR) repertoire in the blood of RV+CFZ-treated patients when material was available for the analysis ($n=9$) within the first two weeks of treatment [24, 25]. All samples were immune-sequenced on a multiplex PCR high-throughput TCR sequencing assay at deep resolution (Supp. Figure 7A). Specifically, we sequenced the variable (TCR β V) and joining (TCR β J) regions in the complementarity-determining region 3 (CDR3) of peripheral blood T cells. We did not observe significant diversity at baseline among responding and non-responding patients (Supp. Figure 7B, C).

Consistent with findings that lower $CD8$ clonality is often associated with better outcomes in cancer [34], we also observed a trend toward significantly lower overall clonality ($p=0.06$) in patients with an objective response versus non-responders (Supp. Figure 7D).

We also observed a strong orthogonal matrix correlation with peripheral blood clonal T cell expansion

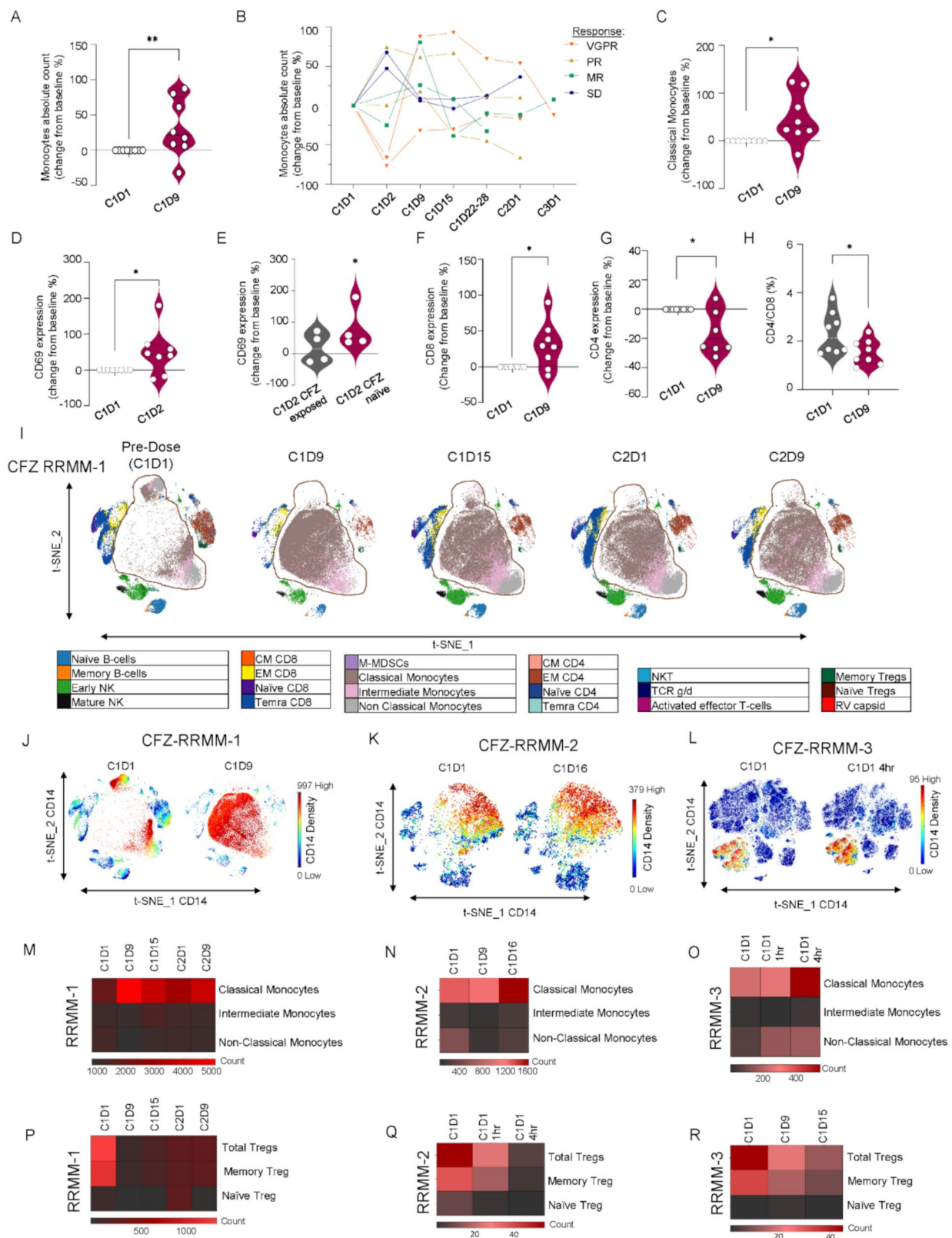


Fig. 5 (See legend on next page.)

(See figure on previous page.)

Fig. 5 RV combined with a PI induces immune activation. **(A)** Violin plots representing multiparametric flow cytometry studies on PB from MM relapsing patients enrolled in RV+CFZ Phase 1b clinical trial, showing overall expansion of total monocytes absolute count (** $p \leq 0.01$) (A); **(B)** Line graphs representing longitudinal multiparametric flow cytometry studies on PB from MM relapsing patients enrolled in RV+CFZ Phase 1b clinical trial, showing overall expansion of total monocytes absolute count. Wilcoxon signed rank p -values: C1D9 > C1D1 p -value = 0.054; **(C-D)** Violin plots representing higher frequency of CD14++ CD16- Classical Monocytes (C) and increase in CD69 activation marker in the total monocytes ($p = 0.047$) (D) on treatment up to the C1D9 compared to baseline C1D1. Statistical analysis was performed following Wilcoxon signed rank p -values, ** $p \leq 0.01$, * $p \leq 0.05$; **(E)** Violin plots representing a slight increase in CD69 activation marker in the PB monocyte compartment of $n = 4$ different patients who were not exposed to CFZ prior the treatment compared to $n = 4$ different patients who instead were CFZ exposed before starting the therapy; **(F-G)** Violin plots highlighting the increased CD8 expression (F) and the decreased CD4 expression (G) up to C1D9. Data are expressed as change from baseline %, Wilcoxon signed rank p -values: * $p \leq 0.05$; **(H)** Violin plot highlighting a decrease in CD4/CD8 ratio from baseline up to C1D9. Data are expressed as change from baseline %, Wilcoxon signed rank p -values: * $p \leq 0.05$; **(I)** In-depth immune profiling of a longitudinal CFZ-resistant patient (RRMM-1) enrolled in RV+CFZ Phase 1b was performed with the Maxpar Direct Immune Profiling System using a dry 30-marker antibody panel. Hierarchical clustering and statistical mapping performed algorithmically via the Cytobank® platform. vi-SNE analysis (iterations = 1000, perplexity = 30) displayed in 2D plots using the resultant t-SNE 1 and t-SNE 2 dimensions. High-fidelity FlowSOM ("self-organizing map") (metacluster = 10 and cluster = 100) based on vi-SNE 2D plots showing 22 immune different immune-compartments; **(J-K-L)** t-SNE heatmap of 3 longitudinal CFZ-resistant patient enrolled in RV+CFZ Phase 1b highlighting expression of selected monocyte population after treatment C1D9 for RRMM-1 (J), C1D16 for RRMM-2 (K), C1D1 for RRMM-3 after 4 h of treatment (L); **(M-N-O)** heatmaps showing absolute count of the different monocyte compartments of 3 longitudinal CFZ-resistant patient enrolled in RV+CFZ Phase 1b; **(P-Q-R)** Heatmaps showing overall distribution of naïve and memory Tregs during the course of the therapy

(Ki-67+T cells) and lower clonality, especially in the two subjects with VGPR (Supp. Figure 6E and Supp. Figure 7E). Although BM aspirates for TCR sequencing were not available, immunohistochemistry of BM core biopsies of patients treated with Pelareorep (Phase 1 trial) [17] alone or Pelareorep+CFZ (Phase 1B) showed that patients treated with the combinatorial therapy had a trend towards higher CD8+T cell BM recruitment on treatment (8.5–26.8% positive cells per high power field, $p = 0.06$), an effect that was not present in patients treated with Pelareorep alone (Fig. 6A, B). To further assess whether the addition of CFZ contributes to support T cell-specific responses against RV-infected cancer cells, we performed TCR sequencing and an ELISpot assay to measure possible changes in the T cell signature induced by the addition of CFZ. Specifically, 2×10^6 5TGM1 cells were intravenously injected in syngeneic C57BL/KaLwRij mice; after 9 days from the injection, mice were randomly divided into four treatment groups. Mice were treated once a week with intravenous injection of RV alone (2×10^7 PFU) ($n = 5$), twice a week with intraperitoneal injection of CFZ (1.6 mg/kg) ($n = 6$), or the combination of both ($n = 6$). Diluent (PBS 1X) treatment of mice was used as control ($n = 8$) (Supp. Figure 7F). Mice were then tested once a week for T cell expansion, and after 3 weeks of treatment the mice were humanely sacrificed and splenocytes and BM cells were isolated (Fig. 6D). TCR sequencing of the T cells isolated from the BM of these mice showed significant lower T cell clonality only in mice treated with RV+CFZ compared to control ($p = 0.009$), RV alone ($p = 0.035$), or CFZ alone ($p = 0.004$) (Fig. 6E). Our data also show that mice treated with RV+CFZ have a higher percentage of circulating effector memory (EM) CD8+T cells when compared to the other treatment groups (Fig. 6F-G). We also found higher IFN- γ production after stimulation with 5TGM1 cells infected with RV (Fig. 6I) of the splenocytes isolated

from mice treated with RV+CFZ, compared to levels in the untreated animals ($p = 0.006$), an effect that was not observed when the mice were treated with RV or CFZ alone in the same experimental conditions (Fig. 6J-K). As expected, no significant IFN- γ production was observed when the same splenocytes were incubated with uninfected 5TGM1 cells (Supp. Figure 7G-H-I), which we used as negative control. These data further support that the addition of CFZ plays a pivotal role in orchestrating T cell responses against viral infected MM cells.

Discussion

Here we report that RV actively infects and replicates in JAM-1(+) circulating monocytes, which in turn deliver active replicative virus to MM cells. Our data provide clear evidence that the anti-viral inflammatory signals in monocytes primarily rely on the NF- κ B activation pathway and that this is almost completely curtailed by the addition of PIs. Although here we primarily focused on the combinatorial activity of CFZ+RV, our data support that this effect can be generalized to different NF- κ B inhibitors, including BTZ and Bay-11, as also recently shown in a Phase 1b trial in which MM patients were instead treated with BTZ+RV [22]. Here for the first time, we show that the addition of a PI strongly improves RV infection and replication in canonical phagocytic monocytes (see Fig. 7 for a mechanistic illustration). These data are aligned with reports showing the importance of NF- κ B activation in monocytes after RNA virus infection, including SARS-CoV-2 and respiratory syncytial virus [35, 36] and are consistent with the well-known anti-MM activity of PIs, which rely on blocking aberrant NF- κ B signals in MM cells [37, 38].

Although PIs have been successfully combined with both immunomodulatory and antibody-based therapies in MM [39], their characterization as immune suppressive drugs have excluded their combination with novel

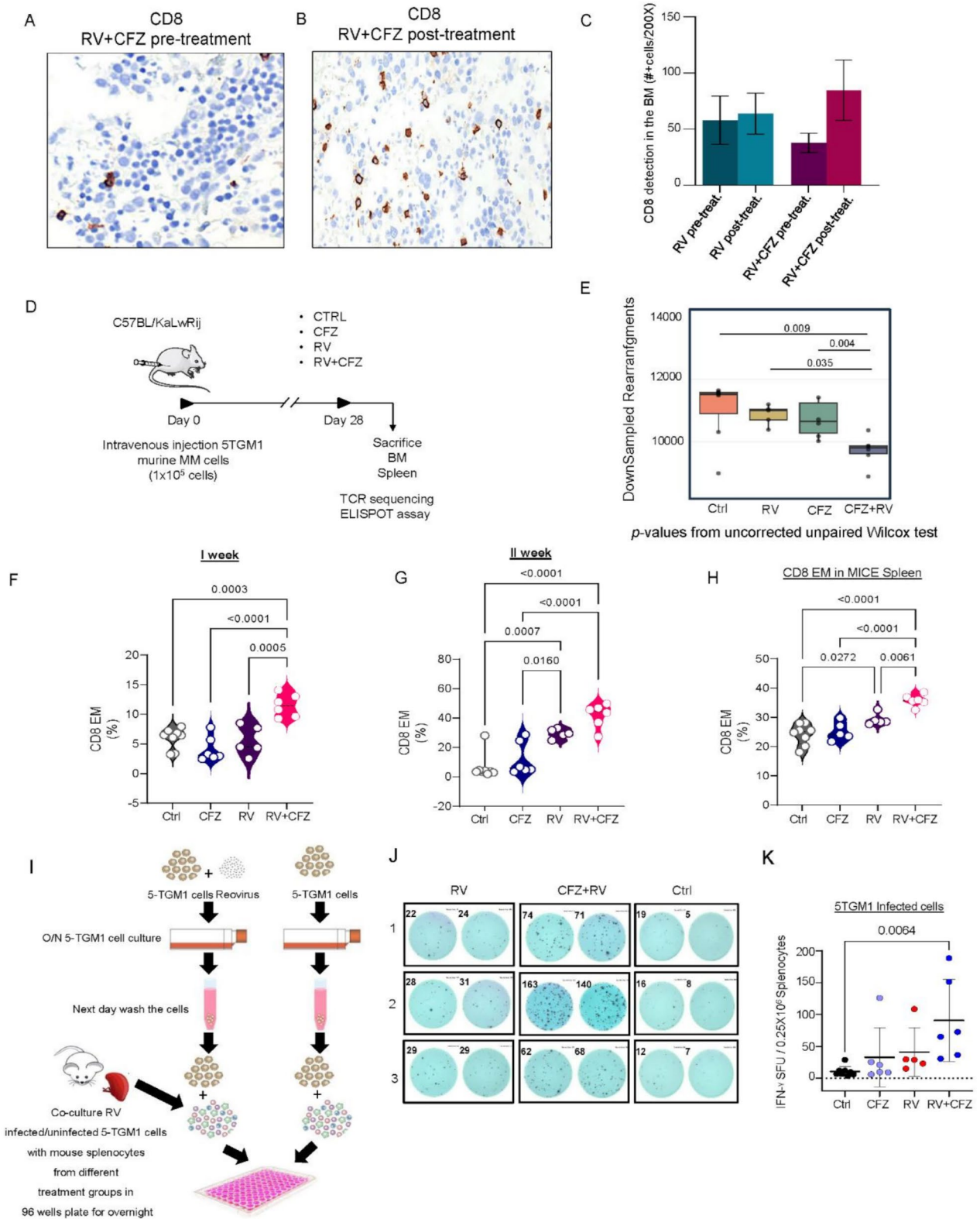


Fig. 6 (See legend on next page.)

(See figure on previous page.)

Fig. 6 RV combined with CFZ treatment promotes T response against MM cells. **(A-B-C)** IHC detection of CD8 protein (signal brown with blue counter-stain) pre **(A)** and post treatment **(B)** in a patient with PR and bar graph in 5 patients following RV monotherapy and combinatorial RV + CFZ. Each value represents the number of positive cells per 200x field. Significant increases were noted in CD8+T cells following treatment with dose level – 1 combination treatment $p=0.060$ **(C)**; **(D)** Immunosequencing of the TCR- β chains using the immunoSEQ Assay from $n=24$ murine BM samples corresponding to 4 different treatment groups (CTRL $n=7$, RV $n=5$, CFZ $n=6$; CFZ + RV $n=6$). **(E)** DS richness, with values indicating that richness of bone marrow samples from RV + CFZ, showed lower richness compared to the other groups. P -values from uncorrected unpaired Wilcoxon test (CTRL vs. RV + CFZ $p=0.009$; RV vs. RV + CFZ $p=0.035$; CFZ vs. RV + CFZ $p=0.004$); **(F-H)** Blood of mice was collected every week to assess circulating CD8+ EM T cells. Violin plot showing CD8+ EM (%) after the first **(F)** and the second **(G)** week of treatment; **(H)** Violin plot showing CD8+ EM T cells in harvested spleen after the treatment; **(I)** Schematic representation of ELISpot assay performed on splenocytes isolated from mice and cocultured ex vivo with 5-TGM-1 infected, or not, with RV (5 MOI) and treated with CFZ alone or in combination. Specifically, after 24 h cells from mouse splenocytes were co-cultured with 5-TGM1 cells (infected with 10 MOI reovirus or uninfected). After 48 h, cells were washed, incubated with biotinylated secondary anti-IFN- γ antibody, and processed for ELISpot Reader System; **(J)** Representative IFN- γ ELISPOT assay plate showing IFN- γ positive spots of splenocytes isolated from treated mice and cocultured ex vivo with 5TGM-1 cells infected with RV and treated or not with CFZ compared to the CTRL group. Wells were imaged using an automated plate-scanner; **(K)** Scatter plots showing numbers of IFN- γ spot forming units (SFUs) after stimulation of splenocytes with 5TGM-1 cells infected with RV

T cell-based therapies. PIs are thought to reduce T cell activity based on preclinical [36] and clinical data showing an increase in the risk for varicella zoster reactivation [40]; the molecular mechanism behind this observation has not yet been characterized.

Here we show, both preclinically and clinically, that blunting the anti-viral inflammatory response with a PI did not impair monocytic activation or T cell activation and expansion upon RV infection, and even increased phagocytic activity of the monocytic fraction against RV-infected MM cells both in *vitro* and *ex-vivo*. In support of our observations recent published data indicated that PI induces MM cell phagocytosis through immunogenic cell death [41]. Hence, in the context of oncolytic viruses, in which delivery to the tumor site is one of the main roadblocks to fully translate their potential anti-cancer benefits into the clinic, the addition of a PI is a logical next step to impair monocytic anti-viral responses and increase viral delivery to the cancer cells, in which higher viral replication and cytolytic activity can be achieved.

Further clinical benefits of adding PIs to viral oncolytic therapies may also derive from their ability not only to potentiate RV infection of cancer cells but also to support RV-induced immune activation in immunosuppressed patients, independently of the PI sensitivity of the cancer cells. The dual immune modulatory effect of PIs may be explained by one or both of the following: (a) the T cell response is mainly driven by the JAK-STAT pathway [42, 43]; (b) PI treatment does not affect IFN- γ release upon viral infection. Of note, recently published data have shown that PI induces anti-viral IFN-I signaling in MM cells [44], mimicking a viral attack, and aligned with these data we observed that in human circulating monocytes PI treatment alone induced transcriptional activation of IFN- α and IFN- β (Supp. Figure 3C and D), but that this induction was significantly lower than what was observed upon RV infection. IFN-I activation signaling upon PI treatment was detected only in the absence of activated NF- κ B pathways by exogenous signals, supporting that PIs can either enhance or impair IFN-I signaling through different signaling pathways and that these two effects

can both contribute to enhance RV-induced killing activity of MM cells. Aligned with Gulla et al. [44], we found that PIs do not impair monocytic or T cell activation, positioning it as an ideal companion drug in the setting of an oncolytic virus or even a T-cell directed therapy such as chimeric antigen directed T-cells or bispecific antibodies targeted to CD3. In fact, the goal in oncolytic virus therapies in both hematological malignancies and solid tumors is to allow maximal infection of tumor cells, and activation of the patient's immune system to clear them once they are infected.

In MM, oncolytic viral therapies are still limited; in fact, despite promising preclinical results with myxoma, varicella, and adenovirus, only an engineered measles virus and reovirus have been given to patients with relapsed MM.

Concerns about intravenous RV injection, or any oncolytic virus, in hematologic malignancies often stem from the abrupt production of antiviral antibodies that are anticipated to neutralize intravenous virus. These common concerns are not supported by several published data showing that immune cells (T cells or dendritic cells) can be loaded with RV ex vivo and administered systemically to deliver virus to tumors, even in the presence of anti-reovirus neutralizing antibodies [45, 46]. In our study we did not find a direct correlation between anti-reovirus neutralizing antibodies and clinical response, which is consistent with our previously published data in which anti-reovirus antibodies were equally found in all treated RV patients [17]. Aligned with these data, results in patients with colorectal liver metastases indicated that free RV delivered systemically could access tumors, and that functional virus was associated with immune cells in the blood but was not found in plasma [28]. Neutralizing antibodies can instead be used by RV to internalize in human CD11b⁺ monocytes, which later can deliver replicative RV to tumor cells, resulting in infection and ultimately lysis [47]. Other published data in an animal model have clearly shown that increasing the frequency of circulating monocytes through GM-CSF treatment enhances delivery and activity of intravenous RV [48],

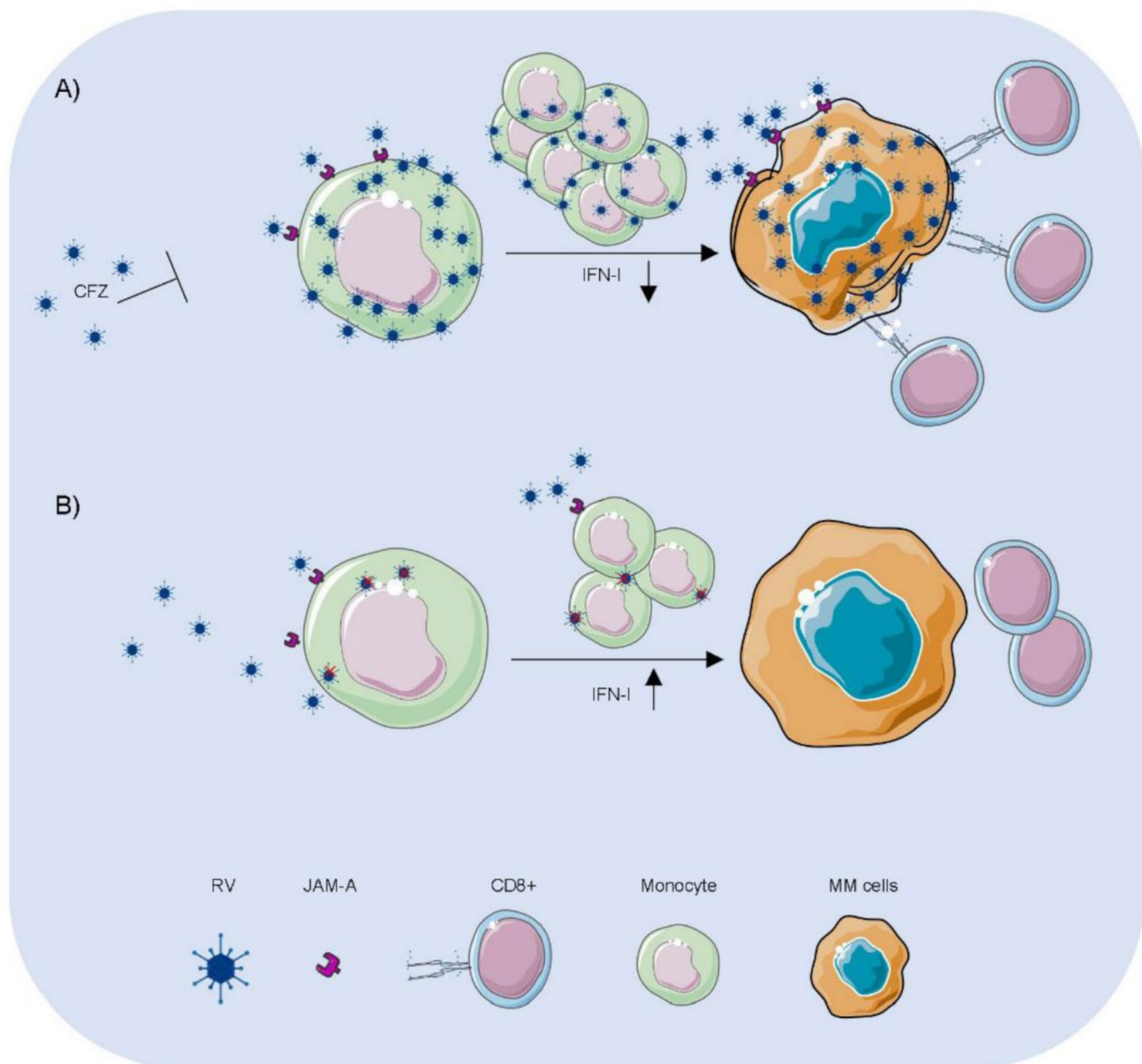


Fig. 7 Graphical abstract illustrating the proposed mechanism of RV combined with CFZ in patients with MM. **(A)** Graphical representation of the proposed mechanism showing how proteasome inhibition (CFZ) increases the viral delivery to MM cells and enhances myeloma oncolytic reovirus therapy by suppressing IFN-I monocytic anti-viral immune responses through monocyte expansion and CD8+ cytotoxic T cell activation against cancer cells; **(B)** Graphical representation of the proposed mechanism of the lack of viral delivery to MM cells in the absence of proteasome inhibition

further supporting that enhancing RV infection of circulating monocytes independently of the presence of neutralizing antibodies may be a successful therapeutic strategy.

Another concern is that non-engineered naturally occurring viruses such as RV are unlikely to be therapeutically active unless partnered with an activating agent. PIs are a rational choice to combine with viruses, as they prevent signaling through NF- κ B in immune cells, abrogating the initial inflammatory antiviral response, even though this effect is short-lived [49]. Nevertheless, most

studies of PIs in combination with an oncolytic virus focus on induction of the unfolded protein response and its potential enhancement of cytotoxic effects [50] or viral replication in vitro [51]. An earlier publication investigating the combination of RV plus the PI BTZ reported that the addition of BTZ enhanced RV-induced apoptosis in MM cells [21]. More recently, the same group has highlighted a possible immune modulatory effect of the RV+BTZ combination in a phase 1b trial [22], an effect that seems to be independent of the synergistic killing activity of these two compounds on the cancer cells as

initially reported [21]. However, the mechanism of action behind these observations has not been investigated. A subsequent publication investigating this combination could not evaluate synergy, as only doses that led to 50% cytotoxicity were used. However, this study emphasized the importance of RV infection of the tumor microenvironmental cells [23]. Our experiments showed that at early time points, PI treatment of MM cells did not enhance viral replication or improve RV-induced apoptosis, but rather showed a decrease in viral replication and non-additive effect on tumor cell killing. This is a result that we believe is consistent with the tendency of viruses to actively replicate and produce viable progeny particles in living host cells rather than in dying cells [27].

Our clinical data clearly show that the addition of a PI plays a pivotal role in supporting active viral replication in the cancer cells *in vitro* and *in vivo*, independently of the PI sensitivity of the MM cells. In our patients treated with combination treatment, viral replication was associated with the presence of both viral genome and viral capsid in the BM and caspase-3 activation, an effect that was not observed in our previous single-agent RV trial. In line with our *ex vivo* testing, patients with MM who were treated with Pelareorep+CFZ showed monocytic and T cell expansion and activation, an immunological and clinical response that was observed even in patients resistant to CFZ, further highlighting the immunomodulatory activity of a PI independent of the direct anti-MM effect. Although these data are strongly aligned with results from a recent BTZ+RV phase 1b trial conducted by another research group [22], which included a mixed population of BTZ sensitive and resistant patients, our *in vitro* data and patient population involve only BTZ- and CFZ-resistant patients. Our results conclusively show that the effect of PI in enhancing RV therapy is instead independent from its direct cytotoxicity activity against MM cells. Although the attribution of a specific clinical response to one agent in a combination therapy can be challenging, our animal data show that addition of a PI is essential to orchestrate T cell responses to RV-infected cancer cells, further supporting the importance of a PI not only in oncolytic viral therapy but also in T cell adaptive immune response, as also recently showed from Gulla et al. [41]. Aligned with Kelly et al. [52], who reported that RV-infected MM cells significantly upregulate the expression of surface PD-L1, we found that the MM cells of Pelareorep+CFZ treated patients have increased PD-L1 expression on their surface compared to patients treated with Pelareorep alone. Although higher PD-L1 expression is a sign of productive MM cell infection, we must also take into consideration that PD-L1 upregulation can negatively impact direct killing of cancer cells by T cells. We believe that, as suggested from Kelly et al., the combination with anti-PD-L1 therapy can

further potentiate the anti-MM activity of Pelareorep, which we plan to explore in combination with CFZ.

Conclusions

Our data are the first to highlight proteasome inhibition as an optimal therapeutic companion to enhance oncolytic virus therapy independently of its direct anti-cancer activity, leading these observations to be relevant not only for MM but also for oncolytic viruses in solid tumors.

Abbreviations

BM	Bone marrow
BMMCs	Bone marrow mononuclear cells
BTZ	Bortezomib
Clo	Clodronate liposomes
CM	Central memory
CTRL	Control liposomes
CFZ	Carfilzomib
CytoF	Cytometry by time of flight
EM	Effector memory
GM-CSF	Granulocyte-macrophage colony-stimulating factor
HSV-1	Herpes simplex virus-1
MM	Multiple myeloma
MNCs	Mononuclear cells
MR	Minimal response
PB	Peripheral blood
PBMCs	Peripheral blood mononuclear cells
PD	Progressive disease
PI	Proteasome inhibitor
PR	Partial response
RV	Reovirus
SD	Stable disease
TEMRA	Terminally differentiated
TVEC	Talimogene laherparepvec
VGPR	Very good partial response

Supplementary Information

The online version contains supplementary material available at <https://doi.org/10.1186/s13045-024-01645-3>.

Supplementary Material 1

Acknowledgements

The authors wish to thank Dr. Domenico Viola and Dr. Francesca Besi for their technical support in our study. The authors also thank Dr. Jacqueline Cloos for providing RPMI-BTZ resistant and sensitive cell lines.

Author contributions

CCH & DWS wrote the clinical protocol, enrolled the patients, analyzed the clinical data, selected primary MM samples analyzed *ex-vivo*, and wrote the portions of the manuscript associated with the clinical data, part of the introduction and discussion. FP and AD wrote the portion of the manuscript associated with the preclinical data and part of the introduction and discussion. JS performed the scientific writing and editing of the manuscript. FP, AD, TT, LN, MS and MMurtadha designed the preclinical experiments. AD, TT, LN, MMurtadha, EC, MMoloudizargari, YZ, PS, ON, and HV performed the preclinical experiments and analyzed the data. AD, TT, JW and MS performed CyTOF experiments and data analysis. AD, TT, LN and EC performed *in vivo* experiments. GM supported the scientific editing of the manuscript. LN performed all the immunofluorescence and electron microscope experiments and data analysis. GN performed all the IHC correlative studies in patients and wrote this part in the manuscript. MC contributed to the TCR-sequencing analysis and data analysis. AC and AP supported the statistical part of the manuscript. All the authors have contributed substantially to revising the manuscript for important content and final approval.

Funding

National Cancer Institute of the National Institutes of Health grant UM1CA186691-06 (PI Taofeek Owonikoko), with the Cancer Therapy Evaluation Program (CTEP) providing Pelareorep (Reolysin). National Cancer Institute grant R01CA194742 (CCH & FP). This research was also supported by the National Institute grant R50-CA252135 (EC). Research reported in this publication included work performed at the City of Hope Analytical Cytometry, Biostatistics and Mathematical Oncology, Hematopoietic Tissue Biorepository, Integrated Mass Spectrometry, Integrative Genomics, Light Microscopy/Digital Imaging, and Small Animal Studies Cores, supported by the National Institutes of Health under award number P30CA033572. The content is solely the responsibility of the authors and does not represent the official views of the National Cancer Institute or the National Institutes of Health. The manuscript was shared with the NCI at NCICTEPpubs@mail.nih.gov and pio@ctep.nci.nih.gov. Ottavio Napolitano is a CIRM Scholar supported by the California Institute for Regenerative Medicine (EDU4-12772).

Data availability

The datasets used and/or analysed during the current study are available from the corresponding authors on reasonable request.

Declarations

Ethics approval and consent to participate

The Ohio State University Cancer Institutional Review Board (Columbus, OH) approved this study, and informed consent was obtained from all enrolled patients (www.clinicaltrials.gov, NCT 02101944). All animal experiments were approved by the City of Hope Institutional Animal Care and Use Committee.

Consent for publication

Not applicable.

Competing interests

GJN received research funding from Oncolytics Biotech Inc. MC is employed by Oncolytics Biotech Inc. CCH received research funding from BMS, Oncolytics Biotech, Sanofi, and Nektar; he received personal funds from GlaxoSmithKline, Oncopeptides, BMS, Janssen, Sanofi, and Celgene for advisory board participation, and patent-related funds from Recursion Pharmaceuticals. DWS received personal funds for consultation and advisory board participation from Sanofi, Janssen, SkylineDx, GlaxoSmithKline, Legend Biotech and Amgen.

Author details

¹Judy and Bernard Briskin Center for Multiple Myeloma Research, Department of Hematology and Hematopoietic Cell Transplantation, City of Hope, Duarte, CA, USA

²Department of Hematologic Malignancies Translational Science, Beckman Research Institute, City of Hope, Duarte, CA, USA

³Department of Computational and Quantitative Medicine, Beckman Research Institute, City of Hope, Duarte, CA, USA

⁴Oncolytics Biotech, Inc., Calgary, Canada

⁵Phylogeny Medical Laboratory, Powell, OH, USA

⁶Division of Hematology and Hematologic Malignancies, University of Utah - Huntsman Cancer Institute, Salt Lake City, UT, USA

⁷Department of Hematology and Medical Oncology, Winship Cancer Institute of Emory University, Atlanta, GA, USA

Received: 5 September 2024 / Accepted: 26 November 2024

Published online: 20 January 2025

References

- Berkrot B. FDA Approves Amgen's Injected Immunotherapy for Melanoma 2015 <http://www.reuters.com/article/2015/10/27/us-amgen-fda-idUSKCN05L2YH20151027>
- Kelly K, Nawrocki S, Mita A, Coffey M, Giles FJ, Mita M. Reovirus-based therapy for cancer. *Expert Opin Biol Ther.* 2009;9(7):817–30.
- Sabin AB, Reoviruses. A new group of respiratory and enteric viruses formerly classified as ECHO type 10 is described. *Science.* 1959;130(3386):1387–9.
- Bouziat R, Hinterleitner R, Brown JJ, Stencel-Baerenwald JE, Ikizler M, Mayassi T, et al. Reovirus infection triggers inflammatory responses to dietary antigens and development of celiac disease. *Science.* 2017;356(6333):44–50.
- Thirukkumaran CM, Shi ZQ, Luider J, Kopciuk K, Gao H, Bahlis N, et al. Reovirus modulates autophagy during oncolysis of multiple myeloma. *Autophagy.* 2013;9(3):413–4.
- Duncan MR, Stanish SM, Cox DC. Differential sensitivity of normal and transformed human cells to reovirus infection. *J Virol.* 1978;28(2):444–9.
- Hashiro G, Loh PC, Yau JT. The preferential cytotoxicity of reovirus for certain transformed cell lines. *Arch Virol.* 1977;54(4):307–15.
- Barton ES, Connolly JL, Forrest JC, Chappell JD, Dermody TS. Utilization of sialic acid as a coreceptor enhances reovirus attachment by multistep adhesion strengthening. *J Biol Chem.* 2001;276(3):2200–11.
- Barton ES, Forrest JC, Connolly JL, Chappell JD, Liu Y, Schnell FJ, et al. Junction adhesion molecule is a receptor for reovirus. *Cell.* 2001;104(3):441–51.
- Gentsch JR, Pacitti AF. Effect of neuraminidase treatment of cells and effect of soluble glycoproteins on type 3 reovirus attachment to murine L cells. *J Virol.* 1985;56(2):356–64.
- Kelly KR, Espitia CM, Zhao W, Wendlandt E, Tricot G, Zhan F, et al. Junctional adhesion molecule-A is overexpressed in advanced multiple myeloma and determines response to oncolytic reovirus. *Oncotarget.* 2015;6(38):41275–89.
- Stiff A, Caserta E, Sborov DW, Nuovo GJ, Mo X, Schlotter SY, et al. Histone deacetylase inhibitors enhance the therapeutic potential of Reovirus in multiple myeloma. *Mol Cancer Ther.* 2016;15(5):830–41.
- Coffey MC, Strong JE, Forsyth PA, Lee PW. Reovirus therapy of tumors with activated Ras pathway. *Science.* 1998;282(5392):1332–4.
- Strong JE, Coffey MC, Tang D, Sabinin P, Lee PW. The molecular basis of viral oncolysis: usurpation of the ras signaling pathway by reovirus. *EMBO J.* 1998;17(12):3351–62.
- Kelly K, Espitia CM, Medina EC, Mahalingam D, Oyajobi BO, Coffey M, Giles FJ, Carew JS, Nawrocki S. Reolysin induces endoplasmic reticular stress in multiple myeloma and enhances the activity of bortezomib. *Eur J Cancer Suppl.* 2010;8(7):183.
- Thirukkumaran CM, Shi ZQ, Luider J, Kopciuk K, Gao H, Bahlis N, et al. Reovirus as a viable therapeutic option for the treatment of multiple myeloma. *Clin cancer Research: Official J Am Association Cancer Res.* 2012;18(18):4962–72.
- Sborov DW, Nuovo GJ, Stiff A, Mace T, Lesinski GB, Benson DM Jr, et al. A phase I trial of single-agent reolysin in patients with relapsed multiple myeloma. *Clin cancer Research: Official J Am Association Cancer Res.* 2014;20(23):5946–55.
- Müller LME, Migneco G, Scott GB, Down J, King S, Askar B et al. Reovirus-induced cell-mediated immunity for the treatment of multiple myeloma within the resistant bone marrow niche. *J Immunother Cancer.* 2021;9(3).
- van de Donk N, Pawlyn C, Yong KL. Multiple myeloma. *Lancet.* 2021;397(10272):410–27.
- Hideshima T, Ikeda H, Chauhan D, Okawa Y, Raje N, Podar K, et al. Bortezomib induces canonical nuclear factor-kappaB activation in multiple myeloma cells. *Blood.* 2009;114(5):1046–52.
- Kelly KR, Espitia CM, Mahalingam D, Oyajobi BO, Coffey M, Giles FJ, et al. Reovirus therapy stimulates endoplasmic reticular stress, NOXA induction, and augments bortezomib-mediated apoptosis in multiple myeloma. *Oncogene.* 2012;31(25):3023–38.
- Nawrocki ST, Olea J, Villa Celli C, Dadrastoussi H, Wu K, Tsao-Wei D, et al. Comprehensive single-cell immune profiling defines the patient multiple myeloma microenvironment following oncolytic virus therapy in a phase Ib trial. *Clin cancer Research: Official J Am Association Cancer Res.* 2023;29(24):5087–103.
- Thirukkumaran CM, Shi ZQ, Nuovo GJ, Luider J, Kopciuk KA, Dong Y, et al. Oncolytic immunotherapy and bortezomib synergy improves survival of refractory multiple myeloma in a preclinical model. *Blood Adv.* 2019;3(5):797–812.
- Robins HS, Campreggher PV, Srivastava SK, Wachter A, Turtle CJ, Khsai O, et al. Comprehensive assessment of T-cell receptor beta-chain diversity in alpha-beta T cells. *Blood.* 2009;114(19):4099–107.
- Carlson CS, Emerson RO, Sherwood AM, Desmarais C, Chung MW, Parsons JM, et al. Using synthetic templates to design an unbiased multiplex PCR assay. *Nat Commun.* 2013;4:2680.
- Robins H, Desmarais C, Matthis J, Livingston R, Andriessen J, Reijonen H, et al. Ultra-sensitive detection of rare T cell clones. *J Immunol Methods.* 2012;375(1–2):14–9.
- Jones JE, Le Sage V, Lakdawala SS. Viral and host heterogeneity and their effects on the viral life cycle. *Nat Rev Microbiol.* 2021;19(4):272–82.

28. Adair RA, Roulstone V, Scott KJ, Morgan R, Nuovo GJ, Fuller M, et al. Cell carriage, delivery, and selective replication of an oncolytic virus in tumor in patients. *Sci Transl Med*. 2012;4(138):138ra77.
29. Zamora PF, Hu L, Knowlton JJ, Lahr RM, Moreno RA, Berman AJ et al. Reovirus nonstructural protein σ NS acts as an RNA stability factor promoting viral genome replication. *J Virol*. 2018;92(15).
30. Ramelyte E, Tastanova A, Balázs Z, Ignatova D, Turko P, Menzel U, et al. Oncolytic virotherapy-mediated anti-tumor response: a single-cell perspective. *Cancer Cell*. 2021;39(3):394–e4064.
31. Clarke P, Meintzer SM, Moffitt LA, Tyler KL. Two distinct phases of virus-induced nuclear factor kappa B regulation enhance tumor necrosis factor-related apoptosis-inducing ligand-mediated apoptosis in virus-infected cells. *J Biol Chem*. 2003;278(20):18092–100.
32. Farone AL, O'Donnell SM, Brooks CS, Young KM, Pierce JM, Wetzel JD, et al. Reovirus strain-dependent inflammatory cytokine responses and replication patterns in a human monocyte cell line. *Viral Immunol*. 2006;19(3):546–57.
33. Rajkumar SV, Harousseau JL, Durie B, Anderson KC, Dimopoulos M, Kyle R, et al. Consensus recommendations for the uniform reporting of clinical trials: report of the International Myeloma Workshop Consensus Panel 1. *Blood*. 2011;117(18):4691–5.
34. Porciello N, Franzese O, D'Ambrosio L, Palermo B, Nisticò P. T-cell repertoire diversity: friend or foe for protective antitumor response? *J Experimental Clin Cancer Research*. CR. 2022;41(1):356.
35. Ennaciri J, Ahmad R, Menezes J. Interaction of monocytic cells with respiratory syncytial virus results in activation of NF-kappaB and PKC-alpha/beta leading to up-regulation of IL-15 gene expression. *J Leukoc Biol*. 2007;81(3):625–31.
36. Kircheis R, Haasbach E, Lueftenegger D, Heyken WT, Ocker M, Planz O. NF-kB pathway as a potential target for treatment of critical stage COVID-19 patients. *Front Immunol*. 2020;11:598444.
37. Demchenko YN, Glebov OK, Zingone A, Keats JJ, Bergsagel PL, Kuehl WM. Classical and/or alternative NF-kappaB pathway activation in multiple myeloma. *Blood*. 2010;115(17):3541–52.
38. Khalife J, Ghose J, Martella M, Viola D, Rocci A, Troadec E et al. MiR-16 regulates crosstalk in NF-kB tolerogenic inflammatory signaling between myeloma cells and bone marrow macrophages. *JCI Insight*. 2019;4(21).
39. Palumbo A, Chanan-Khan A, Weisel K, Nooka AK, Masszi T, Beksac M, et al. Daratumumab, bortezomib, and dexamethasone for multiple myeloma. *N Engl J Med*. 2016;375(8):754–66.
40. Chanan-Khan A, Sonneveld P, Schuster MW, Stadtmauer EA, Facon T, Harousseau JL, et al. Analysis of herpes zoster events among bortezomib-treated patients in the phase III APEX study. *J Clin Oncol*. 2008;26(29):4784–90.
41. Gulla A, Morelli E, Johnstone M, Turi M, Samur MK, Botta C, et al. Loss of GABARAP mediates resistance to immunogenic chemotherapy in multiple myeloma. *Blood*. 2024;143(25):2612–26.
42. Seif F, Khoshmirsafa M, Aazami H, Mohsenzadegan M, Sedighi G, Bahar M. The role of JAK-STAT signaling pathway and its regulators in the fate of T helper cells. *Cell Communication Signaling: CCS*. 2017;15(1):23.
43. Twhogig JP, Cardus Figueras A, Andrews R, Wiede F, Cossins BC, Derrac Soria A, et al. Activation of naïve CD4(+) T cells re-tunes STAT1 signaling to deliver unique cytokine responses in memory CD4(+) T cells. *Nat Immunol*. 2019;20(4):458–70.
44. Gulla A, Morelli E, Samur MK, Botta C, Hideshima T, Bianchi G, et al. Bortezomib induces anti-multiple myeloma immune response mediated by cGAS/STING pathway activation. *Blood Cancer Discovery*. 2021;2(5):468–83.
45. Ilett EJ, Barcena M, Errington-Mais F, Griffin S, Harrington KJ, Pandha HS, et al. Internalization of oncolytic reovirus by human dendritic cell carriers protects the virus from neutralization. *Clin cancer Research: Official J Am Association Cancer Res*. 2011;17(9):2767–76.
46. Ilett EJ, Prestwich RJ, Kottke T, Errington F, Thompson JM, Harrington KJ, et al. Dendritic cells and T cells deliver oncolytic reovirus for tumour killing despite pre-existing anti-viral immunity. *Gene Ther*. 2009;16(5):689–99.
47. Berkeley RA, Steele LP, Mulder AA, van den Wollenberg DJM, Kottke TJ, Thompson J, et al. Antibody-neutralized reovirus is effective in oncolytic virotherapy. *Cancer Immunol Res*. 2018;6(10):1161–73.
48. Ilett E, Kottke T, Donnelly O, Thompson J, Willmon C, Diaz R, et al. Cytokine conditioning enhances systemic delivery and therapy of an oncolytic virus. *Mol Therapy: J Am Soc Gene Therapy*. 2014;22(10):1851–63.
49. Koreth J, Kim HT, Lange PB, Poryanda SJ, Reynolds CG, Rai SC, et al. Bortezomib-based immunosuppression after reduced-intensity conditioning hematopoietic stem cell transplantation: randomized phase II results. *Haematologica*. 2018;103(3):522–30.
50. Marchica V, Franceschi V, Vescovini R, Storti P, Vicario E, Toscani D, et al. Bovine pestivirus is a new alternative virus for multiple myeloma oncolytic virotherapy. *J Hematol Oncol*. 2020;13(1):89.
51. Yoo JY, Jaime-Ramirez AC, Bolyard C, Dai H, Nallanagulari T, Wojton J, et al. Bortezomib treatment sensitizes oncolytic HSV-1-treated tumors to NK cell immunotherapy. *Clin cancer Research: Official J Am Association Cancer Res*. 2016;22(21):5265–76.
52. Kelly KR, Espitia CM, Zhao W, Wu K, Visconte V, Anwer F, et al. Oncolytic reovirus sensitizes multiple myeloma cells to anti-PD-L1 therapy. *Leukemia*. 2018;32(1):230–3.

Publisher's note

Springer Nature remains neutral with regard to jurisdictional claims in published maps and institutional affiliations.